N-cadherin SPRY motifs bind unconventionally-secreted Fbxo45 and regulate multipolar neuron migration

Abbreviated title: N-cadherin, Fbxo45 and multipolar neuron migration

Youn Na[1,3], Elif Kon[2], Hong Cao[1,3], Yves Jossin[2,4], Jonathan A. Cooper[1,4]

[1] Basic Sciences Division, Fred Hutchinson Cancer Research Center, Seattle, Washington, 98019, USA

[2] Laboratory of Mammalian Development & Cell Biology, Institute of Neuroscience, Université catholique de Louvain, 1200 Brussels, Belgium

[3] Present Addresses:

YN; Samsung NeuroLogica, Danvers, MA

HC; Institutes of Brain Science, State Key Laboratory of Medical Neurobiology and Collaborative Innovation Center for Brain Science, Fudan University, 200032, China

[4] Contributing authors

Correspondence: Email: jcooper@fhcrc.org

Number of pages: 40

Number of Figures: 8; Supplementary Tables 3; Supplementary Figures 5

ABSTRACT

During development of the mammalian neocortex, the orientation of migrating multipolar projection neurons is controlled by Reelin, a secreted glycoprotein, which increases cell-surface expression of N-cadherin. Although N-cadherin regulates cell-cell adhesion, recent results suggest that its adhesive function is not required to orient multipolar neuron migration. To understand N-cadherin function in multipolar migration, we performed two independent screens for embryonic brain proteins that bind the N-cadherin extracellular domain. Both screens detected MycBP2 and SPRY-domain protein Fbxo45, two components of an intracellular E3 ubiquitin ligase. We found that Fbxo45 is secreted by a non-classical mechanism, not involving a signal peptide and not requiring endoplasmic reticulum to Golgi transport. Secreted Fbxo45 stimulated neurite branching in culture. A SPRY-motif N-cadherin mutant did not bind Fbxo45 and failed to rescue neuron migration even though it still formed trans-homophilic adhesions. The results suggest that secreted Fbxo45 may regulate neurite branching and bind N-cadherin to orient multipolar neuron migration.

INTRODUCTION

The complex architecture of the mammalian neocortex arises through the generation, specification, migration and connection of different types of neurons (1-3). Projection neurons, born and specified in the pallial ventricular zone (VZ), migrate outwards to form discrete layers before they establish connections. Their migrations pass through discrete stages. They first migrate radially from the VZ to the subventricular zone (sVZ)/intermediate zone (IZ), where they become multipolar and migrate randomly (4). When they arrive in the upper IZ, they assume a bipolar morphology and migrate radially outwards, passing by the earlier-born neurons in the cortical plate (CP) until they stop at the marginal zone (MZ) and undergo terminal somal translocation. Genetic disruption of pathways that regulate neuron migration is associated with neurodevelopmental disorders including lissencephaly, epilepsy and schizophrenia.

Classical cadherins, including neuronal (N-)cadherin (NCad) and epithelial (E-)cadherin (ECad), are calcium-dependent cell-cell adhesion molecules (5). NCad is important for cell-cell adhesion in the neuroepithelium of the VZ (6, 7). Somewhat surprisingly, NCad also regulates projection neuron migration at two stages: first to orient multipolar neurons towards the CP (8-10), and second, for bipolar neurons to undergo terminal translocation (11-13). NCad is upregulated on the cell surface at both these stages in response to an extracellular signal, Reelin. Reelin is known to regulate neuron migration and cortical development by stimulating signaling pathways involving Src kinases, Dab1, PI3' kinase, Crk/CrkL, C3G, and the small GTPase, Rap1 (14-21). Rap1 then regulates NCad surface expression, presumably through Rab GTPase-dependent vesicular trafficking events (9, 11, 22). However, the downstream events by which NCad regulates multipolar neuron migration have not been elucidated.

Because cadherin trans-interactions are critical for cell-cell adhesion and recognition (5), we hypothesized that homophilic interactions between NCad on migrating neurons and NCad on other neurons, axons, or radial glia may orient multipolar migration. Indeed, neurons in culture will polarize towards an external source of NCad (23). However, our recent work

revealed that a NCad^{W161A} mutant, which cannot form "strand-swap" trans homodimers (24-27), stimulates multipolar migration (28). We further found that NCad binds and activates fibroblast growth factor receptors (FGFRs) in cis (on the same cell) and this interaction is needed for multipolar migration (28). ECad is not able to replace NCad for this function even though binds FGFR. Mechanistically, NCad but not ECad protected FGFR from being degraded, and the first two of five extracellular calcium-binding domains on NCad (EC1 and EC2) were critical. These results leave open the possibility that additional proteins binding NCad EC1 or EC2 may regulate neuron migration.

Fbxo45 (F box/SPRY domain-containing protein 1) is a little-studied protein that is highly expressed in the nervous system and required for cortical lamination, axonal outgrowth and synaptic connectivity (29-31). Most F-box proteins bind Skp1, Cul1 and Rbx1 to form a SCF (Skp1-Cul1-F-box) E3 ubiquitin ligase complex. Fbxo45 is atypical in that it does not bind Cul1 or Rbx1 and instead associates with MycBP2/PAM (Myc binding protein 2/protein associated with Myc), forming a Fbxo45-Skp1-MycBP2 complex that has E3 ligase activity in vitro (30). The SPRY domain of Fbxo45 potentially interacts with substrates. Curiously, NCad was detected in a Fbxo45 interaction screen (32). Furthermore, knockdown of Fbxo45 decreased NCad expression and impaired differentiation of neuronal stem cells (32), suggesting that Fbxo45 interaction with NCad is involved in brain development.

Here we set out to identify secreted proteins that interact with the ectodomain of NCad and may regulate radial migration. Two different unbiased proteomics approaches detected Fbxo45 and MycBP2 as major binding partners for the extracellular domain of NCad. We found that the SPRY domain of Fbxo45 binds a SPRY domain consensus in the EC1 region of NCad but not ECad. Furthermore, Fbxo45 is secreted by an unconventional mechanism from neurons and other cells and regulates dendritic arborization in vitro. Cell autonomous knockdown of Fbxo45 interfered with neurogenesis, which precluded analysis of neuron migration. Therefore, we tested the potential role of Fbxo45 in neuron migration by an alternative approach. We

generated a NCad mutant which does not bind to Fbxo45 but still forms calcium-regulated trans-homophilic interactions. Unlike NCad^{W161A}, which binds Fbxo45 and rescues multipolar migration (28), the mutant NCad that does not bind Fbxo45 did not rescue multipolar migration. These results suggest that secreted Fbxo45 may stimulate NCad-dependent neuron migration during brain development.

RESULTS

BioID identifies Fbxo45 and MycBP2 as extracellular NCad-interacting neuronal proteins.

We used two approaches to identify NCad binding proteins. First, we adapted proximity-dependent biotin identification (BioIDf) for extracellular use (33). BioID uses the BirA mutant (R118G, BirA*) to generate reactive biotinyl-AMP from biotin and ATP. Biotinyl-AMP rapidly reacts with nucleophiles in the immediate surroundings, including ε-amino groups of lysine residues on nearby proteins (33). BioID has been used to detect binding partners of relatively insoluble proteins including those at cell junction complexes (34-37). The working distance of BirA* is ~10 nm (34), which is about half the length spanned by the five EC repeats that comprise the NCad ectodomain (38) (diagrammed in Figure 1A). To detect proteins that might interact with either end of the NCad ectodomain, we inserted Myc-BirA* into HA-tagged NCad (NCad-HA) either between EC5 and the transmembrane domain (TM) (N5-BirA*) or in the middle of EC2 (N2-BirA*, Figure 1A). Insertion of small protein domains at these sites does not to interfere with cadherin function (38). As a control, the EC1-5 region of N5-BirA* was replaced with EC1-5 of ECad, to create E5-BirA*.

We first tested whether cadherin BirA* proteins were expressed and trafficked to the surface. Western blotting showed that all BirA* proteins were expressed, contained Myc and HA tags, and transferred biotin to cell proteins when provided with ATP and biotin in the media (Supplementary Figure 1A). Immunofluorescence of cadherin-BirA* fusion proteins confirmed that they were transported to the surface and localized to cell-cell junctions in HEK293 cells,

resembling wildtype NCad (38) (Figure 1A and Supplementary Figure 1B). Moreover, NCad was biotinylated when cells co-transfected with NCad and N5-BirA* were labeled with ATP and biotin (Figure 1B). These results suggest that N5-BirA* is in close proximity to NCad in cell-cell adhesions.

We then used N5-BirA* and N2-BirA* in BioID experiments to identify neuronal proteins that interact with the NCad extracellular domain. Figure 1C shows the experimental design. N5-BirA* and N2-BirA* were expressed in HEK293 cells that were then cultured with rat embryonic cortical neurons and labeled with biotin and ATP. Cell lysates were collected and samples were analyzed for protein expression (top, Figure 1D) and biotinylation (bottom, Figure 1D). The remaining sample was purified using high-affinity Streptavidin beads and digested with trypsin before LC-MS/MS analysis. The experiment was performed twice, once with GFP as a negative control (Experiment 1), and once with E5-BirA* as a negative control (Experiment 2). The peptides that were identified were searched against the human and rat protein databases. Since the neurons originated from rat embryos, we were able to identify neuronal proteins by looking for peptide sequences that differ between rat and human. The top ten rat proteins that were detected with N5-BirA* or N2-BirA* but not with GFP or E5-BirA* in both experiments are listed in Figure 1E, and a full list provided in Table 1. MycBP2 and Fbxo45 were the highest-ranked rat neuron proteins in both experiments (Figure 1E and Supplementary Table 1). MycBP2 also was the highest-ranked human protein in both experiments (Supplementary Table 2). The results suggest that Fbxo45 and MycBP2 are major proteins expressed by rat neurons that interact with the ectodomain of NCad.

Affinity purification of neuronal proteins that bind to NCad.

As an independent approach to detect proteins that might regulate neuron migration, we affinity purified proteins from embryonic mouse brain homogenate using recombinant NCad^{W161A} ectodomain, which does not form strand-swap dimers, as bait. The ectodomain was fused to the

human immunoglobulin constant region (Fc), expressed in HEK293T cells, and purified from the culture supernatant using a Protein A/G (PAG) column. An ECad-Fc fusion protein was prepared similarly as a negative control. Neuronal proteins were then purified as illustrated in Figure 2A. Mouse embryonic forebrains were homogenized, insoluble material was removed by centrifugation, and the supernatant passed over PAG. Flow through from the PAG column was then passed over ECad-Fc, to remove proteins that bind to ECad. The unbound material was then passed over NCad^{W161A}-Fc, to select proteins that bind to NCad^{W161A}. All three columns were washed and eluted at low pH. Samples of various fractions were visualized by silver staining after SDS-PAGE (Figure 2B). As expected, PAG retained large amounts of ~55 and 25 KDa proteins, corresponding in size to immunoglobulin heavy and light chains (IgH and IgL, lane 7). ECad-Fc and NCad^{W161A}-Fc eluates contained a spectrum of proteins of various sizes (lanes 9 and 11), including major amounts of ~110 kDa proteins corresponding to the cadherin-Fc fusions. The ECad-Fc and NCad^{W161A}-Fc eluates were then subjected to preparative SDS polyacrylamide gel electrophoresis and the gel stained with colloidal Coommassie (Supplementary Figure 1C). Gel regions above and below the ~110 KDa cadherin-Fc bands were excised, trypsinized and analyzed by LC-MS/MS. The most abundant proteins that bound to NCad^{W161A} but not to ECad are listed in Figure 2C, and a complete list is provided in Supplementary Table 3. MycBP2 and Fbxo45 were the major proteins. Skp1 was also detected. Both our screens complement the findings of (32), who detected NCad as a major interacting protein for Fbxo45, and are consistent with an extracellular Fbxo45-Skp1-MycBP2 complex.

The EC1-2 region of NCad interacts with the SPRY domain of Fbxo45.

To confirm that Fbxo45 binds to NCad but not ECad, Fbxo45 was tagged with T7 at the N terminus and co-transfected with C-terminally HA-tagged cadherins. As expected, Fbxo45 co-immunoprecipitated with NCad but not ECad (Figure 3A). When the ectodomain of NCad was deleted (ΔEC) or the EC1-2 domains of NCad were switched to ECad (EN), Fbxo45 binding was

inhibited (Figure 3B). Moreover, NCad EC1-2 was sufficient to bind Fbxo45 (Figure 3C). Taken together, our data suggest that the NCad but not ECad EC1-2 domains are necessary and sufficient to bind Fbxo45. This finding is consistent with our observation that Fbxo45 was more efficiently biotinylated if BirA* was fused into EC2 than into the juxtamembrane region (compare N2-BirA* and N5-BirA*, Table 1), and with a previous report (32).

We next investigated the NCad-binding region of Fbxo45. Fbxo45 contains an F-box domain (33-83) and a SPRY domain (92-283), which binds ubiquitin ligase substrates (30). We deleted different regions of the SPRY domain and assayed binding to NCad (Figure 3D). Remarkably, none of the mutants tested was able to bind NCad, even when we deleted as little as 10 residues from the C terminus (mutant 276) or five residues between 225 and 229 (Δ225-229). These regions correspond to beta strands 11 and 15 in the predicted structure of the Fbxo45 SPRY domain (39). Our results implicate the folded structure of the Fbxo45 SPRY domain in binding to NCad.

SPRY-binding motifs in NCad

Since Fbxo45 binds the EC1-2 region of NCad but not ECad (Figure 3), we reasoned that the Fbxo45 SPRY domain makes contact with EC1-2 residues that differ between NCad and ECad. Three sequences resembling the canonical SPRY domain-binding consensus ([DE][IL]NXN (40)) are present in this region, and all three differ between NCad and ECad (Figure 4A). Chung et al (32) previously reported that deletion of motifs 2 and 3 abolished Fbxo45 binding. However, motifs 2 and 3 also fit the calcium-binding consensus (DXNDN (25, 41)) and chelate calcium ions in the NCad ectodomain crystal structure (PDB: 3Q2W (42)). Therefore, deleting motifs 2 and 3 might interfere with calcium-dependent folding and indirectly disrupt Fbxo45 binding. To avoid disrupting calcium binding, we substituted each SPRY motif with the corresponding sequence from ECad, generating NCad mutants NC1, NC2, NC3, NC12 and NC123. These mutants, all tagged with HA, were then tested by co-expression with T7-

Fbxo45 and assaying for co-immunoprecipitation (Figure 4B). Substitution of motif 1 (D242S, I243S, N246E and Q247A) almost completely inhibited interaction, while substitution of motif 2 (M261Q) or motif 3 (V376I and P380A) was less inhibitory. Accordingly, the NC12 and NC123 compound mutants did not bind Fbxo45.

To confirm that SPRY motif substitution did not alter NCad folding or homophilic interactions, we co-expressed HA-tagged NCad wildtype or NC123 with T7-tagged NCad or Fbxo45 and tested for co-immunoprecipitation. The result showed that NC123-HA binds NCad-T7 but not T7-Fbxo45 (Figure 4C). This suggests that NC123 folds normally and can form homophilic interactions. Moreover, NC123 could support calcium-dependent cell-cell adhesion. wildtype or mutant NCad were expressed with a GFP marker in CHO-K1 cells, which lack cadherins (43). Transfected cells were incubated under gentle agitation in the presence or absence of calcium. Calcium-dependent aggregation was stimulated by wildtype NCad but not by $NCad^{W161A}$ (Figure 4D), as expected (26). Importantly, NC123 also stimulated calcium-dependent cell aggregation (Figure 4D and Supplementary Figure 2A). These results confirmed that NC123 can form trans-homophilic interactions and $NCad^{W161A}$ cannot. To investigate whether NC123 can also bind in trans to wildtype NCad, we repeated the cell aggregation assay using two cell populations marked by different fluorescent markers. CHO-K1 cells were separately transfected with $NCad^{WT}$ and GFP, or with $NCad^{WT}$ or mutants and mCherry. Equal numbers of transfected cells were allowed to aggregate with or without calcium. GFP+ $NCad^{WT}$ cells aggregated equally with mCherry+ $NCad^{WT}$ or NC123 but not with $NCad^{W161A}$ cells when calcium was added (Supplementary Figure 2B). These results indicate that NC123 and $NCad^{W161A}$ are complementary mutations, with NC123 binding to NCad but not Fbxo45 and $NCad^{W161A}$ binding to Fbxo45 but not NCad. Thus, the NC123 and $NCad^{W161A}$ mutations completely separate two functions of the NCad extracellular domain.

Fbxo45 reaches the cell surface through a non-classical secretion pathway

The binding of Fbxo45 to EC1-2 of NCad raises the question of how an ostensibly intracellular Fbxo45 reaches the extracellular domain of NCad. When cells are lysed for immunoprecipitation, proteins are released from intracellular compartments, from the cell surface, and from the lumen of secretory compartment, which is topologically outside the cell. We tested whether Fbxo45 is on the cell surface using immunofluorescence of non-permeabilized cells. HeLa cells were co-transfected with Flag-Fbxo45 and GFP-NCad (GFP was inserted between EC5 and TM). Anti-Flag and anti-GFP antibodies were added to non-permeabilized cells to detect Fbxo45 and NCad. Both proteins were detected on the cell surface, with GFP-NCad forming a ring around the cells, more intense at cell-cell junctions, and Flag-Fbxo45 more restricted to patches around the cell periphery (Figure 5A and Supplementary Figure 3). This suggests that Fbxo45 is associated with the outer surface of the cell.

To test whether Fbxo45 also localizes to the surface of neurons, primary mouse hippocampal neurons were transfected with Flag-Fbxo45. GFP was co-transfected to show the cell outlines. Flag-Fbxo45 was detected using anti-Flag antibodies with or without permeabilization (Figure 5B). As expected, Fbxo45 was detected in permeabilized neurons throughout the cytoplasm and neurites. Importantly, Fbxo45 was detected on the surface of non-permeabilized cells, where it formed patches (Figure 5B). The non-uniform distribution may be partly due to inaccessibility of some regions due to overlaying non-transfected neurons, or to uneven binding of Fbxo45 to the surface.

Fbxo45 could be actively secreted from cells or released from damaged cells. Secreted proteins typically contain N-terminal signal sequences for co-translational translocation into the lumen of the endoplasmic reticulum (ER) (44). Fbxo45 lacks a consensus signal peptide, and an N-terminal Flag tag did not inhibit its appearance on the surface (Figure 5). However, some proteins that lack signal peptides are secreted by unconventional mechanisms (45-48). While conventional secretion is inhibited by Brefeldin A (BFA), unconventional secretion is insensitive

to BFA (49). We therefore tested whether BFA inhibits secretion of Fbxo45. As expected, BFA inhibited secretion of a similar-sized N-terminal signal sequence protein, NCad EC1-T7. In contrast, BFA slightly increased secretion of T7-Fbxo45 (Figure 6A). BFA did not induce release of a cytoplasmic protein, tubulin. This suggests that Fbxo45 is secreted by a BFA-insensitive unconventional route.

To test whether untagged, endogenous Fbxo45 is secreted by neurons, primary mouse cortical neurons were incubated with serum-free Neurobasal media with or without BFA for 20-24 hrs. Media were collected and Fbxo45 detected with a specific antibody (32). Fbxo45 but not tubulin was detected in the neuron culture media, and secretion was increased by BFA, suggesting unconventional secretion (Figure 6B).

NCad could potentially bind Fbxo45 in an intracellular vesicle and help ferry Fbxo45 to the surface. Therefore, we tested whether co-expression of NCad with Fbxo45 would stimulate Fbxo45 secretion. For this purpose we used full-length NCad, which travels through the conventional secretion pathway. As a negative control, we used NC123, which does not bind Fbxo45 (Figure 4B). NCad did not affect secretion of T7-Fbxo45 from HeLa cells (Figure 6C), or from CHO-K1 cells, which lack endogenous cadherins (Figure 6D). This suggests that NCad does not regulate Fbxo45 secretion.

Taken together these results suggest that Fbxo45 is secreted by a non-classical, signal-independent pathway, and likely associates with NCad only after it reaches the cell surface.

Extracellular Fbxo45 regulates dendrite arborization.

Since NCad is required for dendrite morphogenesis (50-52), we tested if Fbxo45 regulates dendritic arborization and neurite outgrowth. GFP and vector or GFP and Flag-Fbxo45 were co-transfected into DIV5 hippocampal neurons and fixed 2 days later. Neurites were detected by GFP fluorescence and Flag-Fbxo45 was detected by immunofluorescence of permeabilized cells (Supplementary Figure 4A and 4B). Neurons transfected with GFP and

Fbxo45 showed a slight but significant increase in arborization compared with neurons transfected with GFP alone (Figure 7A-C). Increased branching was statistically significant at 115 µm (p=0.0154) and 125 µm from the cell body (p=0.0015, Two-way ANOVA, Bonferroni's multiple comparison test). There were no significant changes in the number of primary neurites or branches (Figure 7D and 7E). There was also no effect on neurite length (Supplementary Figure 4C and 4D).

We also tested if extracellular Fbxo45 regulates dendritic arborization and neurite outgrowth. Fbxo45 or control medium was prepared by from HEK293 cells that had been transfected with T7-Fbxo45 or control vector, and added to DIV5 hippocampal neurons that had been transfected that day with GFP. On DIV7, after 2 additional days of incubation, neurons were fixed and visualized. Secreted Fbxo45 increased arborization between 20 and 100 µm from the soma (Figure 7F-H). The increase was statistically significant at 25 µm (p= 0.0252), 35 µm (p=0.0045) and 65 µm (p=0.0185) from the soma (Two-way ANOVA, Boneferroni's multiple comparison test). In addition, there were significant increases in the number of branches (p=0.0146, two-tailed t-test, n = 52 for control, n = 51 for secreted Fbxo45, Figure 7I) and the number of neurites (p=0.0211, two-tailed t-test, n = 52 for control, n = 51 for secreted Fbxo45, Figure 7J). However, there was no significant difference in the length of neurites and the mean length of neurites per cell (Supplementary Figure 4E and 4F). We did not observe any effects of secreted Fbox45 on dendritic arborization or neurite outgrowth when added to neurons on DIV3 for 2 days (Supplementary Figure 4G-M), suggesting that the function of secreted Fbxo45 is sensitive to the development stage of the neuron. Taken together, the results suggest that extracellular Fbxo45 can stimulate dendritic arborization and neurite outgrowth in vitro.

Neuron migration through the intermediate zone requires NCad SPRY motifs

Since NCad and NCad^{W161A} rescue migration of multipolar neurons (28) and bind to Fbxo45 (Table 3), we reasoned that NCad interaction with Fbxo45 may stimulate radial

migration. We first tested whether Fbxo45 knockdown or over-expression regulates migration. Fbxo45 knockdown inhibited neurogenesis or viability, so we were unable to test whether Fbxo45 is needed cell-autonomously for migration (data not shown). In contrast, over-expressed Fbxo45 inhibited migration (Supplementary Figure 5). This was unexpected if Fbxo45 interacts with NCad to stimulate migration. Since Fbxo45 is secreted, it is possible that over-expression alters the environment in a way that overwhelms directional information.

As an alternative approach, we asked whether NC123, which binds NCad but not Fbxo45, could support neuron migration in vivo. Rap1 blockade with Rap1GAP inhibits NCad upregulation on the neuron surface and delays migration in the multipolar zone (53). This migration delay can be rescued by over-expressed NCad or NCad^{W161A}. We tested whether NC123 could also rescue the migration delay in this assay. Embryos were electroporated in utero at E14.5 to express GFP, Rap1GAP and NCad-HA or NC123-HA. Three days later, embryos were euthanized and the positions of the GFP-expressing neurons were visualized. As shown in Figure 8A and B, Rap1GAP inhibited neuron migration and this was rescued by NCad, as expected. However, NC123 did not rescue migration, suggesting that NCad Fbxo45-binding site is needed for migration from the IZ to the cortical plate. To confirm that NC123 was expressed in this experiment, sections were stained for the HA tag on NCad-HA and NC123-HA. The wildtype and mutant proteins were expressed at similar levels (Figure 8C). Taken together with the finding that NCad^{W161A}-HA rescues migration (28), these results suggest that NCad interaction with Fbxo45 or other proteins through its SPRY motifs is required to orient multipolar neuron migration.

DISCUSSION

NCad plays important roles during brain development, including stabilizing apical junctional complexes in the ventricular zone, regulating the multipolar to bipolar transition in the intermediate zone, stimulating terminal translocation at the top of the cortical plate, and

coordinating axonal, dendritic and synaptic differentiation (6, 7, 11-13, 22, 53). While many of these functions presumably involve trans-homophilic interactions between NCad molecules on the surfaces of neighboring cells, some may not. Indeed, we recently found that trans-interactions are not needed for NCad to stimulate radial migration in the intermediate zone (28). In that study, we found that NCad binds, stabilizes, and activates fibroblast growth factor receptors (FGFRs), and that FGFR stabilization is needed for neuron migration. In the present study we identified Fbxo45 and MycBP2/PAM as major extracellular NCad-binding partners by two unbiased proteomic approaches. Fbxo45 is expressed in the developing brain and mutation affects cortical layering and axonogenesis (30, 31). MycBP2/PAM has no known role in cortical neuron migration, although it does regulate axonal pathfinding (54). We found that Fbxo45 is secreted by an unconventional mechanism, circumventing the usual ER to Golgi pathway, binds to the cell surface, and stimulates dendritic arborization in vitro. Moreover, a SPRY motif mutant NCad that cannot bind Fbxo45, NC123, but can form trans-homophilic interactions is unable to induce the radial migration of multipolar neurons. NC123 can still bind FGFRs (data not shown) suggesting that NCad may interact with both Fbxo45 and FGFRs during neuron migration.

A previous proteomics screen for Fbxo45-binding proteins detected interaction with the NCad extracellular domain and proposed that the interaction occurred inside the cell, before NCad reached the cell surface (32). However, the question of how Fbxo45, which lacks a classic N-terminal signal sequence, would translocate across the ER membrane and come into contact with the NCad extracellular domain was not addressed. We found that the NCad EC1-2 region is necessary and sufficient to bind Fbxo45 and that Fbxo45 is actively secreted from the cell by a non-classical, signal peptide-independent mechanism that is insensitive to BFA. Several other proteins undergo unconventional secretion, including cytokine interleukin-1 (55), thioredoxin (56), fibroblast growth factors FGF-1 (57) and FGF-2 (58), α-Synuclein (59, 60), Galectins (61), phosphoglucose isomerase/autocrine motility factor (62) and heat shock proteins (48). However, the mechanisms and functions of unconventional secretion are still unclear. The

lack of conserved signals, relatively small amounts of proteins secreted, and apparently different cell-type mechanisms have presented technical challenges (46, 48, 63). One mechanism, known as autophagy-mediated secretion, involves chaperone-mediated autophagy (CMA) to translocate proteins into lysosomes, followed by lysosome fusion with the plasma membrane (64). A loose consensus for CMA targeting contains a glutamine preceded or followed by four residues including at least one basic (K or R), one acidic (D or E), and one hydrophobic (I, L, V or F) residue. Fbxo45 contains such a sequence (residues 225-229: QIGER). However, deleting this sequence did not reproducibly inhibit Fbxo45 secretion (data not shown). It is possible that Fbxo45 secretion involves CMA and that variability in secretion may stem from variable levels of autophagy between experiments.

Because unconventional secretion by-passes the usual ER-Golgi route, Fbxo45 may not come into contact with NCad until after both proteins reach the surface. Indeed, co-overexpressing NCad had no effect on the quantity of Fbxo45 secreted (Figure 6C and 6D). However, Fbxo45 could be detected on the cell surface after secretion (Figure 5). Curiously, the binding was not uniform. Extracellular Fbxo45 formed patches, co-localizing with NCad on parts of the cell surface but not others. It is possible that Fbxo45 is only secreted across sub-regions of the surface and binds immediately to NCad in those regions before it can diffuse. Alternatively, some other molecule may be unevenly distributed and either masks or increases binding of Fbxo45 in those regions. The polarized binding of Fbxo45 may be important for its proposed function in guiding neuronal migration.

Deletion of the entire Fbxo45 SPRY domain was previously found to inhibit Fbxo45-NCad interaction (32). We found that deletion of only five (Δ225-229) or ten (Δ277-286) residues from the SPRY domain of Fbxo45 totally disrupted the interaction with NCad (Figure 3D). These residues comprise parts of the β-sheet structure of the SPRY domain, which is critical for displaying loops that mediate protein-protein interactions (39). One caveat is that these

deletions may have inhibited Fbxo45 secretion, thereby preventing access to the NCad extracellular domain. However, we found that NCad and Fbxo45 bind efficiently in vitro after cell lysis (unpublished results). Therefore, even if a mutant Fbxo45 is not secreted, it should be able to bind NCad in the cell lysate. Taken together, it is likely that Fbxo45 forms a conventional SPRY fold, and contacts SPRY-binding motifs in NCad.

We tested candidate Fbxo45-binding SPRY motifs in NCad by replacing NCad sequences with corresponding ECad sequences. Replacement of residues in motifs 3, 2 and 1 increasingly inhibited Fbxo45 binding without inhibiting cell-cell adhesion. Motif 1 is potentially most interesting, since its replacement strongly inhibits Fbxo45 binding (Figure 4). It lies on the opposite surface of EC1 from the EC1-EC1 interface in the strand-swap NCad dimer (42), so Fbxo45 binding is unlikely to alter NCad dimerization. However, this surface has been implicated in cis interactions between adjacent cadherins on the same membrane (42). Mutations here cause measurable changes in mechanical coupling to the actin cytoskeleton but do not affect cell-cell adhesion (65). The same region of ECad is important for a proposed conformational change involved in inside-out activation (66, 67). Mutation of a nearby residue in ECad is found in some cancers and also inhibits inside-out activation (67). Therefore, trans interactions with Fbxo45 may affect cis interactions between NCad molecules on the same cell or modulate NCad conformational activation.

Previous studies showed that Rap1 activation by Reelin in multipolar neurons increases surface expression of NCad and initiates radial migration (53). In addition, Reelin-dependent increases in NCad stimulate terminal translocation at the top of the cortical plate (11-13). It is challenging to study NCad function in migrating neurons because NCad gene silencing (knock-down) disrupts the neurogenic ventricular zone (6). We therefore evaluated NCad function in migration by inhibiting Rap1 in post-mitotic cells and rescuing with wildtype or mutant NCad. The rescue of migration by NCad^{W161A} (28) suggests that stable NCad-NCad interaction is not required, and raises the possibility that another extracellular protein, like Fbxo45, may be

involved. However, attempts to rescue neuron migration by over-expressing Fbxo45 were unsuccessful because ectopic expression of Fbxo45 alone inhibited migration. This may reflect local saturation of NCad and loss of directional information. Furthermore, gene silencing (knock down) of Fbxo45 decreased the number of migrating neurons, perhaps secondary to altered neurogenesis (32). We therefore generated a NCad mutant that retains homophilic interactions but does not interact with Fbxo45. This mutant, NC123, does not rescue migration. Together, our results suggest that NCad-NCad interaction is neither necessary nor sufficient for migration, and that migration correlates with the ability to bind Fbxo45.

It remains a puzzle that Fbxo45 has intracellular and extracellular functions. Inside the cell, Fbxo45 binds MycBP2 and Skp1 to stimulate ubiquitylation and turnover of Par-4, mTOR, Munc-13 and p73 (31, 68-70). This intracellular function is thought to regulate the epithelial-mesenchymal transition and synaptic function (31, 71). However, Fbxo45 is also secreted and binds to NCad from outside the cell. This allows Fbxo45 to have cell non-autonomous functions. Other unconventionally secreted proteins have different functions inside and outside the cell. Heat shock protein 70 (Hsp70) is an intracellular chaperone, but stress stimulates Hsp70 secretion and extracellular Hsp70 activates macrophages (48, 72). Vasohibins catalyze tubulin detyrosination but when secreted regulate angiogenesis (73, 74). As another example, phosphoglucose isomerase is a key metabolic enzyme, but when secreted it is known as autocrine motility factor and stimulates cell migration by binding to specific cell surface receptors (62). By analogy, we can hypothesize that Fbxo45 is secreted under specific biological conditions and that secreted Fbxo45 regulates NCad non-adhesive functions.

In conclusion, Fbxo45 is secreted by a non-classical mechanism. Outside the cell, it binds to SPRY motifs in EC1-2 of NCad. Mutating these motifs inhibits NCad function in neuron migration without affecting cell-cell adhesion. Therefore, secreted Fbxo45, or a protein with overlapping binding requirements, likely regulates NCad during neuron migration. This suggests

that Fbxo45 has different functions depending on whether it is intra- and extra- cellular. More studies are warranted to characterize the mechanism and function of the secreted form.

EXPERIMENTAL PROCEDURES

BioID and expression plasmid cloning

To generate N5-BirA*, a PCR product of myc-BirA* (35700; Addgene) was ligated into XhoI and SpeI cleaved pCAGIG-mNCad-HA, which contains XhoI and SpeI sites introduced into the region between EC5 and the transmembrane domain (53). GFP-NCad contains GFP inserted at the same position. For N2-BirA* cloning, PCR products of myc-BirA* and NCad EC2 were sequentially ligated to pBluescript II KS (+) and the final insert was ligated to pCAGIG-NCad-HA using EcoRI and KpnI. E5-BirA* was created by ligating a PCR product of murine ECad EC1-5 to the transmembrane and intracellular regions of N5-BirA* using EcoRI and XhoI. The murine ECad template was a kind gift of Masatoshi Takeichi (75). CAGGFP (Addgene) and pCAGCherryFP were used for co-transfection. The NC1, NC2, NC3, NC12 and NC123 mutations were created using standard site-directed mutagenesis using Kapa HiFi DNA polymerase (Kapa Biosystems) according to manufacturer's instructions. Murine Fbxo45 (Harvard Plasmid Database) was inserted to pCAGIG vector possessing T7 tag using BamHI and NotI. Fbxo45 deletion mutants were generated by site-directed mutagenesis. All constructs were confirmed by sequencing.

Cell culture and transfection

HEK293, HeLa and CHO-K1 cells were maintained in Dulbecco's modified Eagle's medium (DMEM) with 10% fetal bovine serum (FBS) and penicillin/streptomycin (100 U/ml) and transfected using Lipofectamine 2000 (Thermo Fisher Scientific) according to the manufacturer's instructions. Unless otherwise stated, transfected cells were incubated 40-48

hours before protein analysis or fixation for immunofluorescence. Cortical neurons from embryonic day 18 (E18) Sprague–Dawley rats (Charles River) or E15.5-16.5 CD-1 mice (Charles River) from were prepared as reported previously (76) and maintained in Neurobasal media with B-27 supplements (Thermo Fisher Scientific). All animal procedures were approved by the Fred Hutchinson Cancer Research Center Institutional Animal Care and Use Committee. Neurons were transfected using Lipofectamine 2000. Hippocampal neurons were prepared as reported previously (76), transfected after 3 or 5 days in vitro (DIV), and fixed 2 days later.

Antibodies

The following antibodies were used: mouse N-cadherin (Thermo Fisher Scientific), HRP conjugated Strepavidin (Jackson ImmunoResearch Laboratories, Inc.), mouse anti-tubulin (Santa Cruz Biotechnology, Inc.), mouse anti-T7 (EMD Millipore), mouse anti-HA (HA.11) (BioLegend), rabbit anti-HA (Bethyl, Montgomery) and mouse Flag M2 (Sigma-Aldrich). Rabbit Fbxo45 antibody was kindly provided by Kojo S. J. Elenitoba-Johnson (University of Pennsylvania).

Immunofluorescence

Cells grown on coverslips were fixed in 4 % paraformaldehyde for 20 min followed by permeabilization with 0.25 % Triton X-100 in PBS for 10 minutes. Coverslips were washed in PBS and blocked for 1 hour in 10 % normal goat serum in PBS and primary antibody was added for overnight at 4 °C. After washing with PBS, Alexa Fluor 568-conjugated secondary antibodies were added for 1 hour. After several PBS rinses, coverslips were mounted in ProLong Gold Antifade Mountant (Thermo Fisher Scientific). All procedures were performed at room temperature unless otherwise specified.

Immunoprecipitation and pull down

Cells were washed with cold PBS two times and harvested in 1% Triton X-100 in PBS with protease/phosphatase inhibitors. The lysates were centrifuged at 14,000 rpm for 15 minutes and supernatant mixed with T7 Tag Antibody Agarose (EMD Millipore) for immunoprecipitation or NeutrAvidin (Thermo Fisher Scientific) for the streptavidin pull down for 2 hours. Agarose beads were washed three times with lysis buffer, eluded with SDS sampling buffer, and analyzed by SDS-PAGE and western blotting.

HEK293-neuron trans-biotinylation (BioID)

HEK293 cells were transfected with pCAG plasmids encoding GFP (experiment 1), E5-BirA* (experiment 2), N5-BirA* or N2-BirA* (both experiments). After 24 hours, transfected cells were detached with 5 mM EDTA in PBS, centrifuged at 1,000 rpm for 5 minutes, suspended in Neurobasal media with 10 % horse serum, penicillin/streptomycin (100 U/ml) and B-27 supplements, and added to rat cortical primary cultures that had been prepared 3 days previously. About 10-18 x 10^6 HEK293 cells were added to 100 x 10^6 rat cortical neurons per sample. After overnight incubation, media were changed to fresh Neurobasal media containing 5 % Horse Serum, penicillin/streptomycin (100 U/ml), B-27 supplements, 50 μM biotin and 1 mM ATP. After 24 hours, mixed cells were washed with cold PBS two times and harvested in 1 % Triton X-100 in PBS buffer with 1 mM EDTA and Complete protease inhibitors (Roche). The lysates were centrifuged at 14,000 rpm for 15 minutes and the supernatant mixed with Strepavidin Sepharose High Performance (Sigma-Aldrich) and rotated for 5 hours at 4 °C. Streptavidin beads were washed three times with Buffer 1 (20 mM Tris-HCl, pH 7.4, 0.1 % NP-40, 1 M NaCl, 5 mM EDTA, pH 8.0) followed by Buffer 2 (2 mM Tris-HCL, pH 7.4, 0.1 % NP-40, 0.5 mM EDTA) and Buffer 3 (1 M urea, 10 mM Tris-HCl, pH 7.4, 0.1 % NP-40, 1 mM EDTA), 2 times each. A final wash was performed with 50 mM Tris-HCl, pH 7.4 to remove urea and detergents. The beads were equilibrated with 50 mM ammonium bicarbonate, pH 8.0 and digested with trypsin overnight at 37 °C with gentle agitation. Additional trypsin was added for a

further 2 hours at 37 °C. Digestion was stopped by adding formic acid to 1 % final concentration. Beads were centrifuged at 4,000 rpm for 2 minutes and the supernatant was transferred to a new tube. Beads were rinsed twice more with water and all supernatants were combined and lyophilized. The peptides were cleaned using ZipTip micro-C18 (Millipore Corporation) and analyzed by LC-MS/MS.

LC-MS/MS analysis for BioID

LC-MS/MS analysis was performed with an Easy-nLC 1000 (Thermo Scientific) coupled to an Orbitrap Elite mass spectrometer (Thermo Scientific). The LC system, configured in a vented format, consisted of a fused-silica nanospray needle (PicoTip™ emitter, 75 µm ID, New Objective) packed in-house with Magic C18 AQ 100Å reverse-phase media (Michrom Bioresources Inc.) (25 cm), and a trap (IntegraFrit Capillary, 100 µm ID, New Objective) containing Magic C18 AQ 200Å (2 cm). The peptide sample was diluted in 10 µL of 2% acetonitrile and 0.1% formic acid in water and 8 µL was loaded onto the column and separated using a two-mobile-phase system consisting of 0.1% formic acid in water (A) and 0.1% acetic acid in acetonitrile (B). A 90 minute gradient from 7% to 35% acetonitrile in 0.1% formic acid at a flow rate of 400 nL/min was used for chromatographic separations. The mass spectrometer was operated in a data-dependent MS/MS mode over the m/z range of 400-1800. The mass resolution was set at 120,000. For each cycle, the 15 most abundant ions from the scan were selected for MS/MS analysis using 35% normalized collision energy. Selected ions were dynamically excluded for 30 seconds.

Cadherin-Fc fusion proteins

DNA sequences encoding the ectodomains of ECad and NCad^{W161A} were PCR amplified and cut with MfeI and AgeI (ECad) or EcoRI and AgeI (NCad) and cloned into a plasmid (pcDNA3.1-ApoER2-Fc (15)) that had been cut EcoRI and AgeI. The murine ECad template was a kind gift

of Masatoshi Takeichi (75) and murine NCad^{W161A} template was from (28). The plasmids were confirmed by sequencing. Fusion proteins were produced in HEK293T cells. For each construct, five 6-cm plates were transfected with a total of 120 µg of DNA using the calcium phosphate method. Media were removed 6 hours later and gently replaced with serum-free DMEM. Two days later, media were harvested and concentrated using Amicon Centricon YM-100 centrifugal filters. Protein concentration and purity were estimated by SDS PAGE with a BSA standard. Approximately 250 µg of each fusion protein was mixed with 250 µL packed volume Protein A/G PLUS-Agarose (Santa Cruz Biotechnology) and unbound proteins washed away using PBS.

Purification of proteins interacting with NCad^{W161A} and not with ECad

Brains from 21 mouse embryos (E16.5) were homogenized with a Dounce homogenizer in a total volume of 8 mL of Buffer A (100 mM NaCl, 20 mM Hepes pH 7.5, 2 mM $CaCl_2$, 0.2 mM EDTA, Complete protease inhibitors) containing 1 % Triton X-100. The homogenate was centrifuged at 10,000 x g for 30 minutes at 4 °C. The supernatant was adjusted to contain 0.3 µg/ml DNaseI and mixed with Protein A/G PLUS-Agarose (120 µL packed volume) in a BioRad "Biospin" mini column for 30 minutes at 4 °C. Unbound material was mixed with ECad-Fc bound to Protein A/G PLUS-Agarose (440 µL packed volume, estimated 220 µg ECad-Fc) for 90 minutes at 4 °C. Unbound material was mixed with NCad^{W161A}-Fc bound to Protein A/G PLUS-Agarose (440 µL packed volume, estimated 220 µg ECad-Fc) for 2 hours at 4 °C. Finally, all three columns were washed eight times with 1 mL Buffer A containing 0.1 % Triton X-100, once with 1 mL of 20 mM Hepes pH 7.5, 2 mM $CaCl_2$ and once with 1 mL of H_2O before eluting twice with 1 mL of 0.1 % formic acid in H_2O. Eluates were neutralized with 100 µL 1 M ammonium bicarbonate, frozen, and lyophilized. Lyophilized proteins were dissolved in SDS-PAGE sample buffer and resolved by SDS-PAGE (BioRad precast 4-15% gradient gel). The gel was stained with Simply Blue Safe Stain (Invitrogen). Sections of the gel above and below the Cadherin-Fc bands were excised and analyzed by trypsin digestion and mass spectrometry. Briefly, the gel

pieces were destained with 25 mM ammonium bicarbonate in 50 % acetonitrile, and subsequently dehydrated using acetonitrile. The protein was digested for overnight with 5 ng/µL trypsin (Promega Corporation) in 50 mM ammonium bicarbonate at 37 °C. The peptides were extracted using 5 % v/v formic acid in water, then with acetonitrile. The pooled extracts were dried under vacuum and cleaned using ZipTip™ C18 (Millipore Corporation) before the subsequent MS analysis.

LC-MS/MS analysis for Affinity Purification

LC-MS/MS analysis was performed with an Eksigent NanoLC-2D system (Eksigent/AB Sciex) coupled to an LTQ Orbitrap mass spectrometer (Thermo Scientific). The LC system configured in a vented format (77) consisted of a fused-silica nanospray needle (PicoTip™ emitter, 75 µm ID, New Objective) packed in-house with Magic C18 AQ 100 Å reverse-phase media (Michrom Bioresources Inc.) (25 cm), and a trap (IntegraFrit™ Capillary, 100 µm ID, New Objective) containing Magic C18 AQ 200Å (2 cm). The peptide sample was diluted in 10 µL of 2 % acetonitrile and 0.1 % formic acid in water and 8 µL was loaded onto the column and separated using a two-mobile-phase system consisting of 0.1 % formic acid in water (A) and 0.1 % acetic acid in acetonitrile (B). A 60 min gradient from 7 % to 35 % acetonitrile in 0.1 % formic acid at a flow rate of 400 nL/min was used for chromatographic separations. The mass spectrometer was operated in a data-dependent MS/MS mode over the m/z range of 400-1800. The mass resolution was set at 60,000. For each cycle, the 5 most abundant ions from the scan were selected for MS/MS analysis using 35 % normalized collision energy. Selected ions were dynamically excluded for 45 s.

MS data analysis

Data analysis was performed using Proteome Discoverer 1.4 (Thermo Scientific). The data were searched against Uniprot human (March 19, 2014), rat (January 9, 2015), and mouse (March

19, 2014) protein databases, and against common contaminants (http://www.thegpm.org/crap/). Trypsin was set as the enzyme with maximum missed cleavages set to 2. The precursor ion tolerance was set to 10 ppm, and the fragment ion tolerance was set to 0.6 Da. SEQUEST (78) was used for search, and search results were run through Percolator (79) for scoring.

Preparation of secreted proteins and total cell lysates

To collect secreted proteins, cells were incubated in serum-free DMEM (for HeLa) or Neurobasal Media (for primary cortical neurons) for 20-24 hours at 37 °C with 5 % CO_2. The conditioned medium was centrifuged at 3,000 rpm for 5 minutes to remove cell debris. Supernatants were collected and concentrated using Amicon Ultra, 10 kDa NMWL (EMD Millipore). After removing the conditioned medium, cells were washed with cold PBS and harvested in 1% Triton X-100 in PBS buffer with protease/phosphatase inhibitors. Triton-insoluble material was removed at 14,000 rpm for 15 minutes. Samples of the conditioned medium and cell lysate were analyzed by SDS polyacrylamide gel electrophoresis and Western blotting.

Short-term aggregation assay

CHO-K1 cells were co-transfected with GFP or mCherry and indicated NCad constructs. After 24 hours, transfected cells were washed twice with pre-warmed HCMF (137 mM NaCl, 5.4 mM KCl, 0.63 mM Na_2HPO_4, 5.5 mM Glucose, 10 mM HEPES, pH 7.4) and placed in suspension using 0.01 % trypsin, 1 mM $CaCl_2$ in HCMF. Suspended cells were centrifuged at 1,000 rpm for 5 minutes, resuspended in 0.5 % soybean trypsin inhibitor in HCMF, then washed three times with cold HCMF and counted. 200,000 cells in HCMF were added to 1 % BSA-coated 24-well plates with and without 2 mM $CaCl_2$. Cells were shaken at 80 rpm for 20 minutes at 37 °C and images were collected using 2X or 4X objectives. Cell aggregation assays were performed three biological replicates. Data were quantified using Analyze Particles in Image J (80).

In utero electroporation

In utero microinjection and electroporation was performed at E14.5 essentially as described (81) using timed pregnant CD-1 mice (Charles River Laboratories). In brief, mice were anesthetized and the midline incision the uterine horns were exposed. Plasmid solution was injected into the lateral ventricle using needles for injection that were pulled from Wiretrol II glass capillaries (Drummond Scientific) and calibrated for 1-μl injections. DNA solutions were mixed in 10 mM Tris, pH 8.0 with 0.01% Fast Green. The embryo in the uterus was placed between the forceps-type electrodes (Nepagene) with 5-mm pads and electroporated with five 50-ms pulses of 45 V using the ECM830 electroporation system (Harvard Apparatus). The uterine horns were then placed back into the abdominal cavity to continue normal brain development. Three days later, mice were euthanized and embryo brains were sectioned and GFP visualized. Immunohistochemistry to detect HA-tagged NCad was performed essentially as described (53).

Dendrite Morphology

Images of GFP-expressing mouse hippocampal neurons were acquired as a z-stack (3 sections, 0.5 um per section) on the Deltavision deconvolution microscope (GE Life Sciences,). A maximum intensity projection was created from the z-stack. Images were converted to binary and analyzed using the Sholl Analysis Plugin (82) with the concentric ring size of 10 μm. Intersections between dendrites and each concentric ring were counted. Metamorph Neurite Outgrowth Module (Molecular Devices, Sunnyvale, CA) was used for neurite outgrowth analysis.

Statistical analysis

SUPPLEMENTARY FIGURE LEGENDS

Supplementary Figure 1, related to Figure 1.

Controls for BioID and affinity purification mass spectrometry.

(A) NCad or cadherin-BirA* fusion proteins were expressed in HeLa cells and incubated with or without biotin. Cell lysates were collected and blotted with HA or Myc antibodies or strepavidin as indicated. (B) Low power images of Figure 1A. Enlarged images of the inner square were shown in Figure 1A. Scale bar: 20 μm. (C) Preparative SDS polyacrylamide gel used for protein identification by affinity chromatography. The lanes correspond to samples 8, 9 (duplicate lanes), 11 (duplicate lanes) and 10 of Figure 2A. The gel was stained with colloidal Coommassie Blue (Simple Blue, BioRad). The boxes indicate regions excised for protein identification by LC-MS/MS.

Supplementary Figure 2, related to Figure 4.

NC123 mutant supports homophilic interaction.

(A) Quantification of replicate CHO-K1 aggregation assays shown in Figure 4D. N_0: particle number at time 0 min, N_{20}: particle number at time 20 min. n = 6. ***p <0.001.

(B) Aggregation assay with two different cell populations to investigate trans-interaction between NCad wildtype and mutants. Green cells, co-expressing NCad wildtype and GFP, were mixed with red cells, co-expressing NCad wildtype or mutants and mCherry. Scale bar: 400 μm.

Supplementary Figure 3, related to Figure 5.

Sub-cellular localization of Fbxo45.

(A) Low power images of non-permeabilized HeLa cells. Enlarged images of the inner square were shown in Figure 5A. Scale bar: 20 μm. (B-C) GFP-NCad and Flag-Fbxo45 were co-transfected and immunofluorescence was performed using Flag antibody after permeabilization.

Statistical analysis was performed with GraphPad Prism 7.0 (La Jolla, CA). Statistical significance was determined by two-tailed unpaired t-test or two-way ANOVA followed by the Bonferroni's multiple-comparison test as described in the text. Data are reported as mean±SEM and the statistical significance was set as $p<0.05$.

AUTHOR CONTRIBUTIONS

Y.N., E.K, H.C. and Y.J. performed experiments with technical assistance from J.A.C.

Y.N. and J.A.C. wrote and revised the manuscript with input from Y.J.

ACKNOWLEDGEMENTS

We are very grateful to Barry Gumbiner and Kojo S. J. Elenitoba-Johnson for helpful discussions and sharing reagents. We thank staff of the Fred Hutch shared resources, especially Phil Gafken, Yuko Ogata and Julio Vazquez, for proteomics and imaging; Alexander (Sasha) Straight for technical assistance, and members of the Cooper laboratory for encouragement. This work was supported by grants R01 NS080194 and GM109463 from the U.S. Public Health Service and grants J.0129.15, J.0179.16 and T.0243.18 from the FNRS. FHCRC imaging and proteomics laboratories are supported by P01 CA015704.

1. Marin O, Rubenstein JL. 2003. Cell migration in the forebrain. Annu Rev Neurosci 26:441-83.
2. Bielas S, Higginbotham H, Koizumi H, Tanaka T, Gleeson JG. 2004. Cortical neuronal migration mutants suggest separate but intersecting pathways. Annu Rev Cell Dev Biol 20:593-618.
3. Ayala R, Shu T, Tsai LH. 2007. Trekking across the brain: the journey of neuronal migration. Cell 128:29-43.
4. Kriegstein AR, Noctor SC. 2004. Patterns of neuronal migration in the embryonic cortex. Trends Neurosci 27:392-9.
5. Takeichi M. 1990. Cadherins: a molecular family important in selective cell-cell adhesion. Annu Rev Biochem 59:237-52.
6. Kadowaki M, Nakamura S, Machon O, Krauss S, Radice GL, Takeichi M. 2007. N-cadherin mediates cortical organization in the mouse brain. Dev Biol 304:22-33.
7. Takeichi M, Inuzuka H, Shimamura K, Matsunaga M, Nose A. 1990. Cadherin-mediated cell-cell adhesion and neurogenesis. Neurosci Res Suppl 13:S92-6.
8. Cooper JA. 2014. Molecules and mechanisms that regulate multipolar migration in the intermediate zone. Frontiers in Cellular Neuroscience 8.
9. Jossin Y. 2011. Polarization of migrating cortical neurons by Rap1 and N-cadherin: Revisiting the model for the Reelin signaling pathway. Small GTPases 2:322-328.
10. Gartner A, Fornasiero EF, Valtorta F, Dotti CG. 2014. Distinct temporal hierarchies in membrane and cytoskeleton dynamics precede the morphological polarization of developing neurons. J Cell Sci 127:4409-19.
11. Franco SJ, Martinez-Garay I, Gil-Sanz C, Harkins-Perry SR, Muller U. 2011. Reelin regulates cadherin function via Dab1/Rap1 to control neuronal migration and lamination in the neocortex. Neuron 69:482-97.
12. Gil-Sanz C, Franco SJ, Martinez-Garay I, Espinosa A, Harkins-Perry S, Muller U. 2013. Cajal-Retzius cells instruct neuronal migration by coincidence signaling between secreted and contact-dependent guidance cues. Neuron 79:461-77.
13. Martinez-Garay I, Gil-Sanz C, Franco SJ, Espinosa A, Molnar Z, Mueller U. 2016. Cadherin 2/4 signaling via PTP1B and catenins is crucial for nucleokinesis during radial neuronal migration in the neocortex. Development 143:2121-34.
14. Howell BW, Herrick TM, Cooper JA. 1999. Reelin-induced tyrosine phosphorylation of disabled 1 during neuronal positioning. Genes Dev 13:643-8.

15. Hiesberger T, Trommsdorff M, Howell BW, Goffinet A, Mumby MC, Cooper JA, Herz J. 1999. Direct binding of Reelin to VLDL receptor and ApoE receptor 2 induces tyrosine phosphorylation of disabled-1 and modulates tau phosphorylation. Neuron 24:481-9.
16. Ballif BA, Arnaud L, Arthur WT, Guris D, Imamoto A, Cooper JA. 2004. Activation of a Dab1/CrkL/C3G/Rap1 pathway in Reelin-stimulated neurons. Curr Biol 14:606-10.
17. Park TJ, Curran T. 2008. Crk and Crk-like play essential overlapping roles downstream of disabled-1 in the Reelin pathway. J Neurosci 28:13551-62.
18. Voss AK, Britto JM, Dixon MP, Sheikh BN, Collin C, Tan SS, Thomas T. 2008. C3G regulates cortical neuron migration, preplate splitting and radial glial cell attachment. Development 135:2139-49.
19. Beffert U, Morfini G, Bock HH, Reyna H, Brady ST, Herz J. 2002. Reelin-mediated signaling locally regulates protein kinase B/Akt and glycogen synthase kinase 3beta. J Biol Chem 277:49958-64.
20. Hirota Y, Nakajima K. 2017. Control of Neuronal Migration and Aggregation by Reelin Signaling in the Developing Cerebral Cortex. Front Cell Dev Biol 5:40.
21. Shah B, Lutter D, Tsytsyura Y, Glyvuk N, Sakakibara A, Klingauf J, Puschel AW. 2017. Rap1 GTPases Are Master Regulators of Neural Cell Polarity in the Developing Neocortex. Cereb Cortex 27:1253-1269.
22. Kawauchi T, Sekine K, Shikanai M, Chihama K, Tomita K, Kubo K, Nakajima K, Nabeshima Y, Hoshino M. 2010. Rab GTPases-dependent endocytic pathways regulate neuronal migration and maturation through N-cadherin trafficking. Neuron 67:588-602.
23. Gartner A, Fornasiero EF, Munck S, Vennekens K, Seuntjens E, Huttner WB, Valtorta F, Dotti CG. 2012. N-cadherin specifies first asymmetry in developing neurons. EMBO J 31:1893-903.
24. Pertz O, Bozic D, Koch AW, Fauser C, Brancaccio A, Engel J. 1999. A new crystal structure, Ca^{2+} dependence and mutational analysis reveal molecular details of E-cadherin homoassociation. EMBO J 18:1738-47.
25. Shapiro L, Fannon AM, Kwong PD, Thompson A, Lehmann MS, Grubel G, Legrand JF, Als-Nielsen J, Colman DR, Hendrickson WA. 1995. Structural basis of cell-cell adhesion by cadherins. Nature 374:327-37.
26. Tamura K, Shan WS, Hendrickson WA, Colman DR, Shapiro L. 1998. Structure-function analysis of cell adhesion by neural (N-) cadherin. Neuron 20:1153-63.

27. Boggon TJ, Murray J, Chappuis-Flament S, Wong E, Gumbiner BM, Shapiro L. 2002. C-cadherin ectodomain structure and implications for cell adhesion mechanisms. Science 296:1308-13.
28. Kon E, Calvo-Jimenez E, Cossard A, Na Y, Cooper JA, Jossin Y. 2019. N-cadherin-regulated FGFR ubiquitination and degradation control mammalian neocortical projection neuron migration. eLife 8:e47673.
29. Yoshida K. 2005. Characterization of estrogen-induced F-box protein FBXO45. Oncol Rep 14:531-5.
30. Saiga T, Fukuda T, Matsumoto M, Tada H, Okano HJ, Okano H, Nakayama KI. 2009. Fbxo45 forms a novel ubiquitin ligase complex and is required for neuronal development. Mol Cell Biol 29:3529-43.
31. Tada H, Okano HJ, Takagi H, Shibata S, Yao I, Matsumoto M, Saiga T, Nakayama KI, Kashima H, Takahashi T, Setou M, Okano H. 2010. Fbxo45, a novel ubiquitin ligase, regulates synaptic activity. J Biol Chem 285:3840-9.
32. Chung FZ, Sahasrabuddhe AA, Ma K, Chen X, Basrur V, Lim MS, Elenitoba-Johnson KS. 2014. Fbxo45 inhibits calcium-sensitive proteolysis of N-cadherin and promotes neuronal differentiation. J Biol Chem 289:28448-59.
33. Roux KJ, Kim DI, Raida M, Burke B. 2012. A promiscuous biotin ligase fusion protein identifies proximal and interacting proteins in mammalian cells. J Cell Biol 196:801-10.
34. Kim DI, Birendra KC, Zhu W, Motamedchaboki K, Doye V, Roux KJ. 2014. Probing nuclear pore complex architecture with proximity-dependent biotinylation. Proc Natl Acad Sci U S A 111:E2453-61.
35. Van Itallie CM, Aponte A, Tietgens AJ, Gucek M, Fredriksson K, Anderson JM. 2013. The N and C termini of ZO-1 are surrounded by distinct proteins and functional protein networks. J Biol Chem 288:13775-88.
36. Van Itallie CM, Tietgens AJ, Aponte A, Fredriksson K, Fanning AS, Gucek M, Anderson JM. 2014. Biotin ligase tagging identifies proteins proximal to E-cadherin, including lipoma preferred partner, a regulator of epithelial cell-cell and cell-substrate adhesion. J Cell Sci 127:885-95.
37. Steed E, Elbediwy A, Vacca B, Dupasquier S, Hemkemeyer SA, Suddason T, Costa AC, Beaudry JB, Zihni C, Gallagher E, Pierreux CE, Balda MS, Matter K. 2014. MarvelD3 couples tight junctions to the MEKK1-JNK pathway to regulate cell behavior and survival. J Cell Biol 204:821-38.

38. Kim SA, Tai CY, Mok LP, Mosser EA, Schuman EM. 2011. Calcium-dependent dynamics of cadherin interactions at cell-cell junctions. Proc Natl Acad Sci U S A 108:9857-62.
39. Woo JS, Suh HY, Park SY, Oh BH. 2006. Structural basis for protein recognition by B30.2/SPRY domains. Mol Cell 24:967-76.
40. Kuang Z, Lewis RS, Curtis JM, Zhan Y, Saunders BM, Babon JJ, Kolesnik TB, Low A, Masters SL, Willson TA, Kedzierski L, Yao S, Handman E, Norton RS, Nicholson SE. 2010. The SPRY domain-containing SOCS box protein SPSB2 targets iNOS for proteasomal degradation. J Cell Biol 190:129-41.
41. Patel SD, Ciatto C, Chen CP, Bahna F, Rajebhosale M, Arkus N, Schieren I, Jessell TM, Honig B, Price SR, Shapiro L. 2006. Type II cadherin ectodomain structures: implications for classical cadherin specificity. Cell 124:1255-68.
42. Harrison OJ, Jin X, Hong S, Bahna F, Ahlsen G, Brasch J, Wu Y, Vendome J, Felsovalyi K, Hampton CM, Troyanovsky RB, Ben-Shaul A, Frank J, Troyanovsky SM, Shapiro L, Honig B. 2011. The extracellular architecture of adherens junctions revealed by crystal structures of type I cadherins. Structure 19:244-56.
43. Emond MR, Biswas S, Blevins CJ, Jontes JD. 2011. A complex of Protocadherin-19 and N-cadherin mediates a novel mechanism of cell adhesion. J Cell Biol 195:1115-21.
44. Viotti C. 2016. ER to Golgi-Dependent Protein Secretion: The Conventional Pathway. Methods Mol Biol 1459:3-29.
45. Nickel W, Rabouille C. 2009. Mechanisms of regulated unconventional protein secretion. Nat Rev Mol Cell Biol 10:148-55.
46. Malhotra V. 2013. Unconventional protein secretion: an evolving mechanism. EMBO J 32:1660-4.
47. Nickel W, Seedorf M. 2008. Unconventional mechanisms of protein transport to the cell surface of eukaryotic cells. Annu Rev Cell Dev Biol 24:287-308.
48. De Maio A. 2011. Extracellular heat shock proteins, cellular export vesicles, and the Stress Observation System: a form of communication during injury, infection, and cell damage. It is never known how far a controversial finding will go! Dedicated to Ferruccio Ritossa. Cell Stress Chaperones 16:235-49.
49. Misumi Y, Misumi Y, Miki K, Takatsuki A, Tamura G, Ikehara Y. 1986. Novel blockade by brefeldin A of intracellular transport of secretory proteins in cultured rat hepatocytes. J Biol Chem 261:11398-403.

50. Seong E, Yuan L, Arikkath J. 2015. Cadherins and catenins in dendrite and synapse morphogenesis. Cell Adh Migr 9:202-13.
51. Arikkath J. 2012. Molecular mechanisms of dendrite morphogenesis. Front Cell Neurosci 6:61.
52. Tan ZJ, Peng Y, Song HL, Zheng JJ, Yu X. 2010. N-cadherin-dependent neuron-neuron interaction is required for the maintenance of activity-induced dendrite growth. Proc Natl Acad Sci U S A 107:9873-8.
53. Jossin Y, Cooper JA. 2011. Reelin, Rap1 and N-cadherin orient the migration of multipolar neurons in the developing neocortex. Nat Neurosci 14:697-703.
54. Bloom AJ, Miller BR, Sanes JR, DiAntonio A. 2007. The requirement for Phr1 in CNS axon tract formation reveals the corticostriatal boundary as a choice point for cortical axons. Genes Dev 21:2593-606.
55. Auron PE, Webb AC, Rosenwasser LJ, Mucci SF, Rich A, Wolff SM, Dinarello CA. 1984. Nucleotide sequence of human monocyte interleukin 1 precursor cDNA. Proc Natl Acad Sci U S A 81:7907-11.
56. Rubartelli A, Bajetto A, Allavena G, Wollman E, Sitia R. 1992. Secretion of thioredoxin by normal and neoplastic cells through a leaderless secretory pathway. J Biol Chem 267:24161-4.
57. Jackson A, Friedman S, Zhan X, Engleka KA, Forough R, Maciag T. 1992. Heat shock induces the release of fibroblast growth factor 1 from NIH 3T3 cells. Proc Natl Acad Sci U S A 89:10691-5.
58. Mignatti P, Morimoto T, Rifkin DB. 1992. Basic fibroblast growth factor, a protein devoid of secretory signal sequence, is released by cells via a pathway independent of the endoplasmic reticulum-Golgi complex. J Cell Physiol 151:81-93.
59. Lee HJ, Patel S, Lee SJ. 2005. Intravesicular localization and exocytosis of alpha-synuclein and its aggregates. J Neurosci 25:6016-24.
60. Ahn KJ, Paik SR, Chung KC, Kim J. 2006. Amino acid sequence motifs and mechanistic features of the membrane translocation of alpha-synuclein. J Neurochem 97:265-79.
61. Sato S, Burdett I, Hughes RC. 1993. Secretion of the baby hamster kidney 30-kDa galactose-binding lectin from polarized and nonpolarized cells: a pathway independent of the endoplasmic reticulum-Golgi complex. Exp Cell Res 207:8-18.
62. Funasaka T, Raz A. 2007. The role of autocrine motility factor in tumor and tumor microenvironment. Cancer Metastasis Rev 26:725-35.

63. Nickel W. 2003. The mystery of nonclassical protein secretion. A current view on cargo proteins and potential export routes. Eur J Biochem 270:2109-19.
64. Kaushik S, Cuervo AM. 2012. Chaperone-mediated autophagy: a unique way to enter the lysosome world. Trends Cell Biol 22:407-17.
65. Strale PO, Duchesne L, Peyret G, Montel L, Nguyen T, Png E, Tampe R, Troyanovsky S, Henon S, Ladoux B, Mege RM. 2015. The formation of ordered nanoclusters controls cadherin anchoring to actin and cell-cell contact fluidity. J Cell Biol 210:1033.
66. Petrova YI, Spano MM, Gumbiner BM. 2012. Conformational epitopes at cadherin calcium-binding sites and p120-catenin phosphorylation regulate cell adhesion. Mol Biol Cell 23:2092-108.
67. Petrova YI, Schecterson L, Gumbiner BM. 2016. Roles for E-cadherin cell surface regulation in cancer. Mol Biol Cell 27:3233-3244.
68. Han S, Kim S, Bahl S, Li L, Burande CF, Smith N, James M, Beauchamp RL, Bhide P, DiAntonio A, Ramesh V. 2012. The E3 ubiquitin ligase protein associated with Myc (Pam) regulates mammalian/mechanistic target of rapamycin complex 1 (mTORC1) signaling in vivo through N- and C-terminal domains. J Biol Chem 287:30063-72.
69. Peschiaroli A, Scialpi F, Bernassola F, Pagano M, Melino G. 2009. The F-box protein FBXO45 promotes the proteasome-dependent degradation of p73. Oncogene 28:3157-66.
70. Chen X, Sahasrabuddhe AA, Szankasi P, Chung F, Basrur V, Rangnekar VM, Pagano M, Lim MS, Elenitoba-Johnson KS. 2014. Fbxo45-mediated degradation of the tumor-suppressor Par-4 regulates cancer cell survival. Cell Death Differ 21:1535-45.
71. Diaz VM, de Herreros AG. 2016. F-box proteins: Keeping the epithelial-to-mesenchymal transition (EMT) in check. Semin Cancer Biol 36:71-9.
72. Vega VL, Rodriguez-Silva M, Frey T, Gehrmann M, Diaz JC, Steinem C, Multhoff G, Arispe N, De Maio A. 2008. Hsp70 translocates into the plasma membrane after stress and is released into the extracellular environment in a membrane-associated form that activates macrophages. J Immunol 180:4299-307.
73. Nieuwenhuis J, Adamopoulos A, Bleijerveld OB, Mazouzi A, Stickel E, Celie P, Altelaar M, Knipscheer P, Perrakis A, Blomen VA, Brummelkamp TR. 2017. Vasohibins encode tubulin detyrosinating activity. Science 358:1453-1456.
74. Aillaud C, Bosc C, Peris L, Bosson A, Heemeryck P, Van Dijk J, Le Friec J, Boulan B, Vossier F, Sanman LE, Syed S, Amara N, Coute Y, Lafanechere L, Denarier E, Delphin C, Pelletier L, Humbert S, Bogyo M, Andrieux A, Rogowski K, Moutin MJ. 2017.

Vasohibins/SVBP are tubulin carboxypeptidases (TCPs) that regulate neuron differentiation. Science 358:1448-1453.

75. Nose A, Nagafuchi A, Takeichi M. 1988. Expressed recombinant cadherins mediate cell sorting in model systems. Cell 54:993-1001.
76. Rumbaugh G, Sia GM, Garner CC, Huganir RL. 2003. Synapse-associated protein-97 isoform-specific regulation of surface AMPA receptors and synaptic function in cultured neurons. J Neurosci 23:4567-76.
77. Licklider LJ, Thoreen CC, Peng J, Gygi SP. 2002. Automation of nanoscale microcapillary liquid chromatography-tandem mass spectrometry with a vented column. Anal Chem 74:3076-83.
78. Eng JK, McCormack AL, Yates JR. 1994. An approach to correlate tandem mass spectral data of peptides with amino acid sequences in a protein database. J Am Soc Mass Spectrom 5:976-89.
79. Kall L, Canterbury JD, Weston J, Noble WS, MacCoss MJ. 2007. Semi-supervised learning for peptide identification from shotgun proteomics datasets. Nat Methods 4:923-5.
80. Schneider CA, Rasband WS, Eliceiri KW. 2012. NIH Image to ImageJ: 25 years of image analysis. Nat Methods 9:671-5.
81. Tabata H, Nakajima K. 2008. Labeling embryonic mouse central nervous system cells by in utero electroporation. Dev Growth Differ 50:507-11.
82. Ferreira TA, Blackman AV, Oyrer J, Jayabal S, Chung AJ, Watt AJ, Sjostrom PJ, van Meyel DJ. 2014. Neuronal morphometry directly from bitmap images. Nat Methods 11:982-4.

FIGURE LEGENDS

Figure 1. Characterization of BirA*fusion proteins and BioID screen for NCad *trans*-interacting proteins.

(A) Diagrams of cadherin fusion proteins. All constructs are C-terminally tagged with the HA epitope. NCad, ECad and myc-BirA* are marked blue, green and red. Bottom row shows representative immunofluorescence images of the respective constructs expressed in HEK293 cells. Scale bar: 10 μm. (B) Biotinylation of NCad by N5-BirA*. HEK293 cells were transfected with NCad, N5-BirA*, or NCad and N5-BirA*. Biotinylated NCad was detected with NCad antibody after pulling down biotinylated proteins using Neutravidin beads. Biotinylated proteins in total cell lysates (TCL) were detected using streptavidin-HRP or NCad antibody. (C) Schematic of BioID screen for neuronal proteins that interact with NCad extracellular region. HEK293 cells were transfected with the indicated constructs then co-cultured with DIV3 rat cortical neurons in the presence of biotin and ATP. Cell lysates were purified using Streptavidin beads. (D) Samples were analyzed by Western blotting with anti-HA to detect the fusion proteins and Streptavidin-HRP to detect biotinylated proteins. (E) Samples were analyzed by on-bead trypsin digestion and LC-MS/MS. The table shows the highest abundance rat neuron proteins (peptide spectrum matches) biotinylated in the presence of HEK cells expressing N5-BirA* and N2-BirA* in two experiments, and their corresponding abundance in control samples biotinylated in the presence of HEK cells expressing negative control constructs, GFP (experiment 1) or E5-BirA* (experiment 2). -, undetected.

Figure 2. Affinity purification screen for brain proteins that bind the NCad but not ECad extracellular domain.

(A) Schematic of affinity chromatography purification of embryonic brain proteins that bind to $NCad^{W161A}$ but not ECad. Numbers in parentheses correspond to samples analyzed by SDS polyacrylamide gel electrophoresis. (B) Samples from the purification were analyzed by SDS

polyacrylamide electrophoresis and proteins detected using silver staining. BSA was loaded as a standard. (C) Proteins retained on ECad-Fc PAG (fraction 8) and NCad^{W161A}-Fc PAG (fraction 10) were separated by preparative SDS polyacrylamide gel electrophoresis and regions above and below the cadherin-Fc band excised. Proteins in these regions were analyzed by in-gel trypsin digestion and identified by LC-MS/MS. The table shows the highest abundance mouse proteins (peptide-spectrum matches) detected on NCad^{W161A}-Fc and their corresponding abundance on ECad-Fc. -, undetected; PAG, protein A/G Sepharose.

Figure 3. NCad EC1-2 interacts with SPRY domain of Fbxo45.

(A-C) Various forms of NCad (tagged with HA at the C-terminus) were co-transfected with Fbxo45 (tagged with T7 at the N-terminus) into HeLa cells. Cell lysates were immunoprecipitated with T7 antibody and samples of cell lysates (TCL) and immunoprecipitates analyzed by Western blotting. (A) Fbxo45 interacts with NCad, but not ECad. (B) NCad EC1-2 is necessary to interact with Fbxo45. (C) NCad EC1-2 is sufficient to interact with Fbxo45. (D) SPRY domain of Fbxo45 is necessary to interact with NCad. All deletion mutations in the SPRY domain disrupt Fbxo45 binding to NCad.

Figure 4. SPRY motifs in NCad bind Fbxo45.

(A) Alignment of mouse NCad and ECad EC1-2 sequences. The alignments start with the first residues of the cleaved cadherins, while the numbering corresponds to the primary translation products. Three matches to the SPRY recognition motif ([DE][IL]NXN) in NCad are indicated as Motifs 1-3. Note that motifs 2 and 3 also bind calcium. * indicates W161, which is critical for the strand-swapped trans dimer. (B) Identification of the Fbxo45 binding site. NCad-HA vectors containing ECad residues from motifs 1, 2 or 3, were co-transfected into HeLa cells with T7-Fbxo45. Cell lysates were immunoprecipitated using T7-antibody. (C) NC123 fails to bind Fbxo45 but still binds to NCad. (D) NCad wildtype (WT) and NC123 support calcium-dependent

cell aggregation, while NCad^{W161A} does not. The indicated constructs were transfected into CHO-K1 cells together with GFP as a marker for transfected cells. Scale bar: 800 μm. See quantification of replicate experiments in Supplementary Figure 2.

Figure 5. Fbxo45 associates with the outside of the cell.

(A) GFP-NCad and Flag-Fbxo45 were co-expressed in HeLa cells. Cells were fixed but not permeabilized and stained with antibodies to GFP and Flag. Scale bar: 10 μm. (B) GFP and Flag-Fbxo45 were transfected into hippocampal neurons after 5 days in culture (DIV5). Two days later, cells were fixed and either permeabilized or not permeabilized immunofluorescent staining was performed with Flag antibody. Right hand panels show magnifications of the boxed areas. Scale bar: 20 μm.

Figure 6. Fbxo45 is secreted by an unconventional pathway.

(A) T7-Fbxo45 secretion is secreted by a Brefeldin A (BFA)-insensitive route. HeLa cells were transfected with NCad EC1-T7 or T7-Fbxo45 and incubated with various concentrations of BFA in serum-free media for 24 hours. Cell lysates (TCL) and concentrated media (Media) were harvested. 0.5 % of theTCL and 15 % of the Media were analyzed by Western blotting. (B) Mouse primary cortical neurons secrete Fbxo45 by an unconventional pathway. DIV 2 cultures were incubated with serum-free Neurobasal media containing 0 or 0.1 μg/ml of BFA for 20-24 hours. Media and TCL were subject to Western blotting for Fbxo45 and tubulin (as a control for cell lysis). Ponceau staining shows the equal amount of media was loaded for western. (C, D) Co-expression of NCad or NC123 with Fbxo45 does not affect Fbxo45 secretion by HeLa cells (C) or NCad null CHO-K1 cells (D).

Figure 7. Fbxo45 increases dendritic arborization.

(A, B) Neurons transfected with GFP or GFP and Flag-Fbxo45 after 5 days in vitro (DIV) were visualized on DIV7. Scale bar: 20 μm. (C) Sholl analysis using 10 μm concentric circles around the soma. Error bar shows the mean ± S.E.M. of three biologically independent experiments. *p <0.05. (Two-way ANOVA, Bonferroni's multiple comparison test). (D, E) Total number of neurites and branches. Mean ± S.E.M. of three biologically independent experiments. *p <0.05. (two-tails, unpaired t test).

(F, G) Neurons transfected with GFP on DIV5 were incubated in the presence of control media or media containing secreted T7-Fbxo45 for a further 2 days. GFP-expressing neurons were then visualized. (H) Sholl analysis as in (C), except that the results are from five independent experiments. (I, J) Total number of neurites and branches as in (D, E), except from five independent experiments.

Figure 8. SPRY- motifs in NCad are required for multipolar migration in vivo.

E15.5 mouse embryos were microinjected and electroporated in utero with plasmids expressing GFP alone (control) or Rap1GAP plus vector, NCad or NC123. Two days later, sections were prepared and the positions of GFP-expressing neurons in the developing cortex were recorded. (A) Representative sections. Expressing Rap1GAP inhibited migration in the multipolar migration zone (MMZ). Migration into the radial migration zone (RMZ) was rescued by co-expressing NCad but not NC123. (B) Quantification based on counting GFP-expressing neurons in the multiple sections from multiple embryos. N, number of embryos; VZ, ventricular zone. (C) NCad and NC123 are expressed at similar level by in utero electroporation. Sections of embryo brains electroporated with plasmids expressing Cherry fluorescent protein and either NCad-HA (upper) or NC123-HA (lower) were visualized with anti-HA antibody.

Figure 1

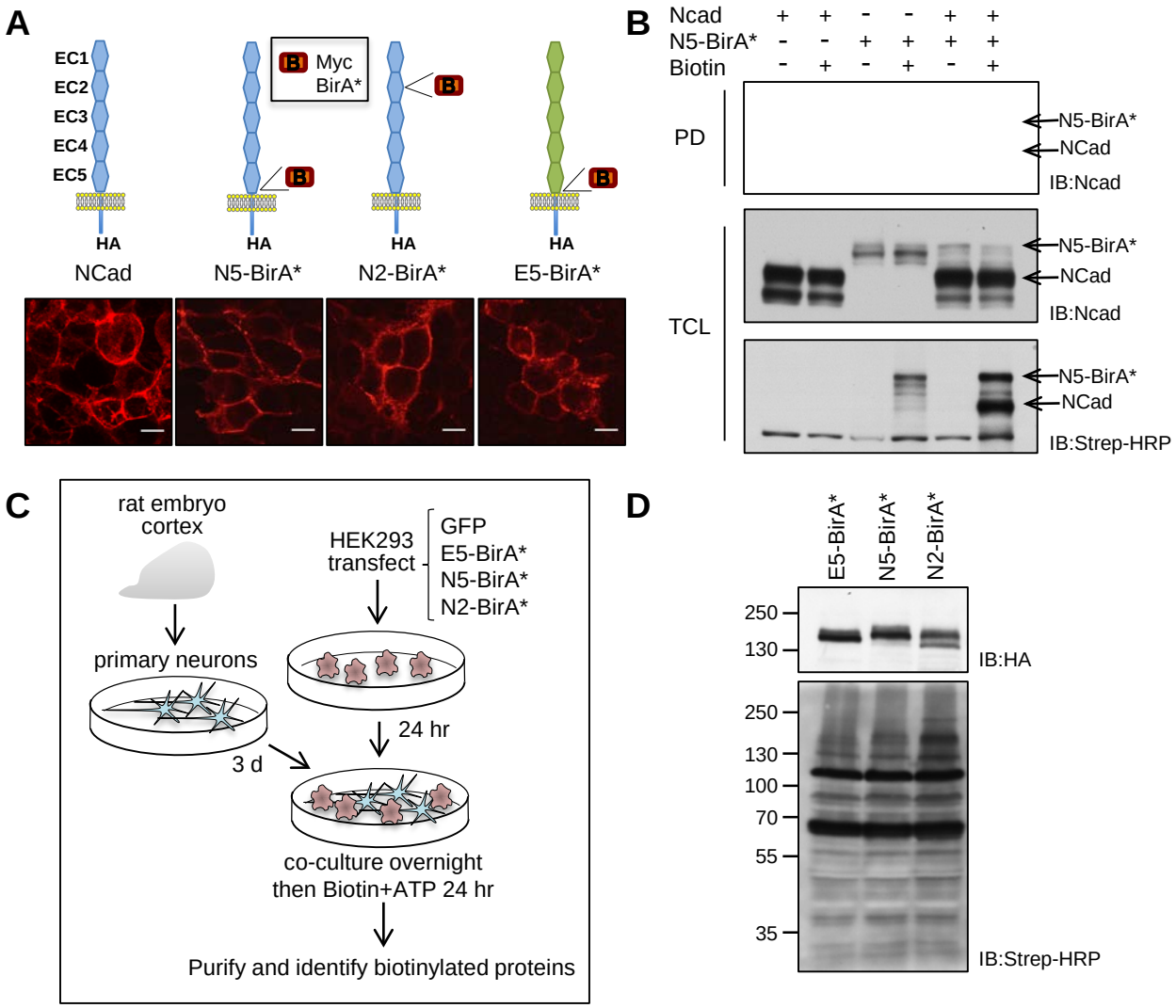

E

Rat Protein	Experiment 1			Experiment 2		
	GFP	N5-BirA*	N2-BirA*	E5-BirA*	N5-BirA*	N2-BirA*
Mycbp2	-	26.15	49.91	-	26.88	46.08
Fbxo45	-	2.99	8.48	-	2.99	8.65
Gramd4	-	2.93	3.10	-	-	6.01
Lamb1	-	-	8.00	-	-	5.51
Scaper	-	-	2.13	-	2.51	5.50
Pex6	-	-	8.77	-	-	5.19
Ndufa5	-	2.67	-	-	-	3.38
C1qbp	-	3.58	-	-	3.13	3.32
Rpp14	-	-	2.94	-	4.36	3.16
Mrpl51	-	-	3.47	-	3.34	2.94

Figure 2

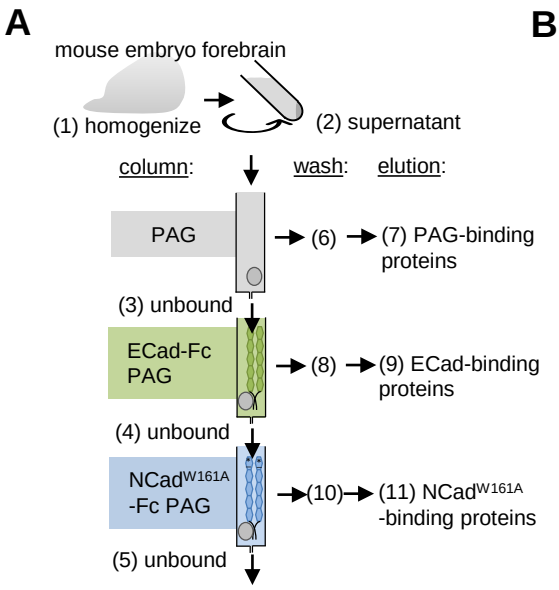

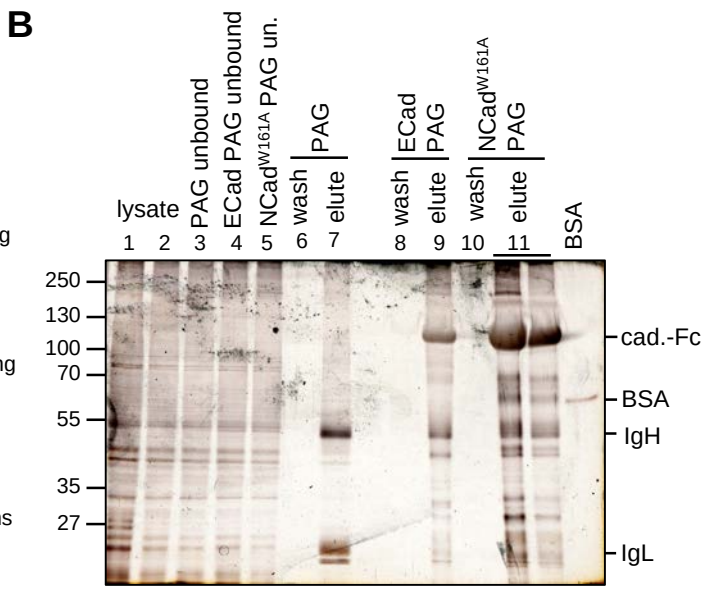

C

Protein	Ecad-Fc	Ncad^{W161A}-Fc
Mycbp2	-	205.37
Fbxo45	-	27.50
Tor2a	-	21.99
Rae1	-	13.51
Spsb2	-	12.70
Tceb1	-	10.66
Pdhb	-	9.71
Skp1	-	7.54
Paics	-	7.10

Figure 3

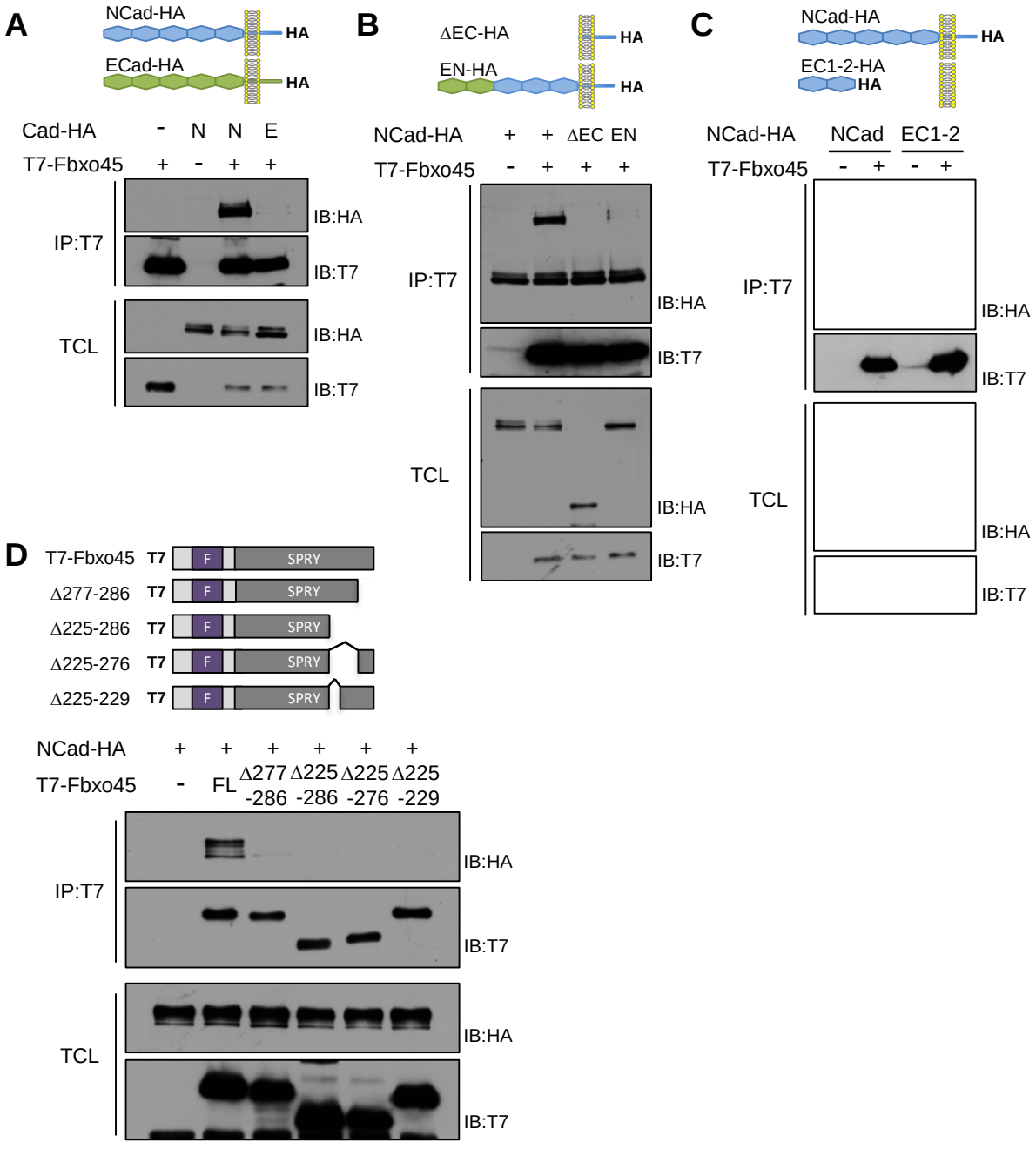
A
NCad-HA
HA
ECad-HA
HA
Cad-HA - N N E
T7-Fbxo45 + - + +
IP:T7
IB:HA
IB:T7
TCL
IB:HA
IB:T7
B
ΔEC-HA
HA
EN-HA
HA
NCad-HA + + ΔEC EN
T7-Fbxo45 - + + +
IP:T7
IB:HA
IB:T7
TCL
IB:HA
IB:T7
C
NCad-HA
HA
EC1-2-HA
HA
NCad-HA NCad EC1-2
T7-Fbxo45 - + - +
IP:T7
IB:HA
IB:T7
TCL
IB:HA
IB:T7
D
T7-Fbxo45 T7 F SPRY
Δ277-286 T7 F SPRY
Δ225-286 T7 F SPRY
Δ225-276 T7 F SPRY
Δ225-229 T7 F SPRY
NCad-HA + + + + + +
T7-Fbxo45 - FL Δ277-286 Δ225-286 Δ225-276 Δ225-229
IP:T7
IB:HA
IB:T7
TCL
IB:HA
IB:T7

Figure 4

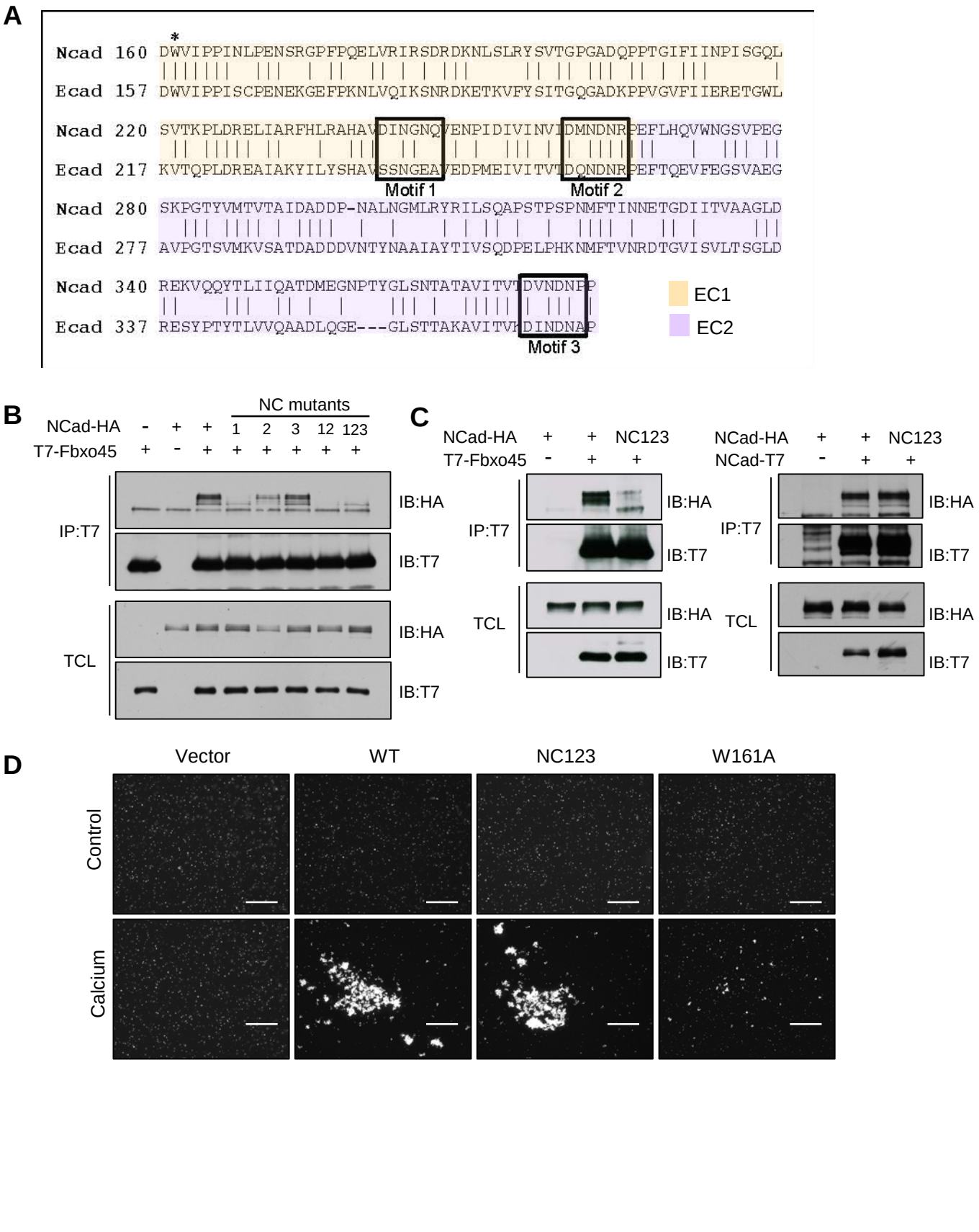
A
Ncad 160 DWVIPPINLPENSRGPFPQELVRIRSDRDKNLSLRYSVTGPGADQPPTGIFIINPISGQL
Ecad 157 DWVIPPISCPENEKGEFPKNLVQIKSNRDKETKVFYSITGQGADKPPVGVFIIERETGWL
Ncad 220 SVTKPLDRELIARFHLRAHAVDINGNQVENPIDIVINVIDMNDNRPEFLHQVWNGSVPEG
Ecad 217 KVTQPLDREAIAKYILYSHAVSSNGEAVEDPMEIVITVTDQNDNRPEFTQEVFEGSVAEG
Motif 1
Motif 2
Ncad 280 SKPGTYVMTVTAIDADDP-NALNGMLRYRILSQAPSTPSPNMFTINNETGDIITVAAGLD
Ecad 277 AVPGTSVMKVSATDADDDVNTYNAAIAYTIVSQDPELPHKNMFTVNRDTGVISVLTSGLD
Ncad 340 REKVQQYTLIIQATDMEGNPTYGLSNTATAVITVTDVNDNPP
Ecad 337 RESYPTYTLVVQAADLQGE---GLSTTAKAVITVKDINDNAP
Motif 3
EC1
EC2
B
NC mutants
NCad-HA - + + 1 2 3 12 123
T7-Fbxo45 + - + + + + + +
IP:T7
IB:HA
IB:T7
TCL
IB:HA
IB:T7
C
NCad-HA + + NC123
T7-Fbxo45 - + +
IP:T7
IB:HA
IB:T7
TCL
IB:HA
IB:T7
NCad-HA + + NC123
NCad-T7 - + +
IP:T7
IB:HA
IB:T7
TCL
IB:HA
IB:T7
D
Vector
WT
NC123
W161A
Control
Calcium

Figure 5

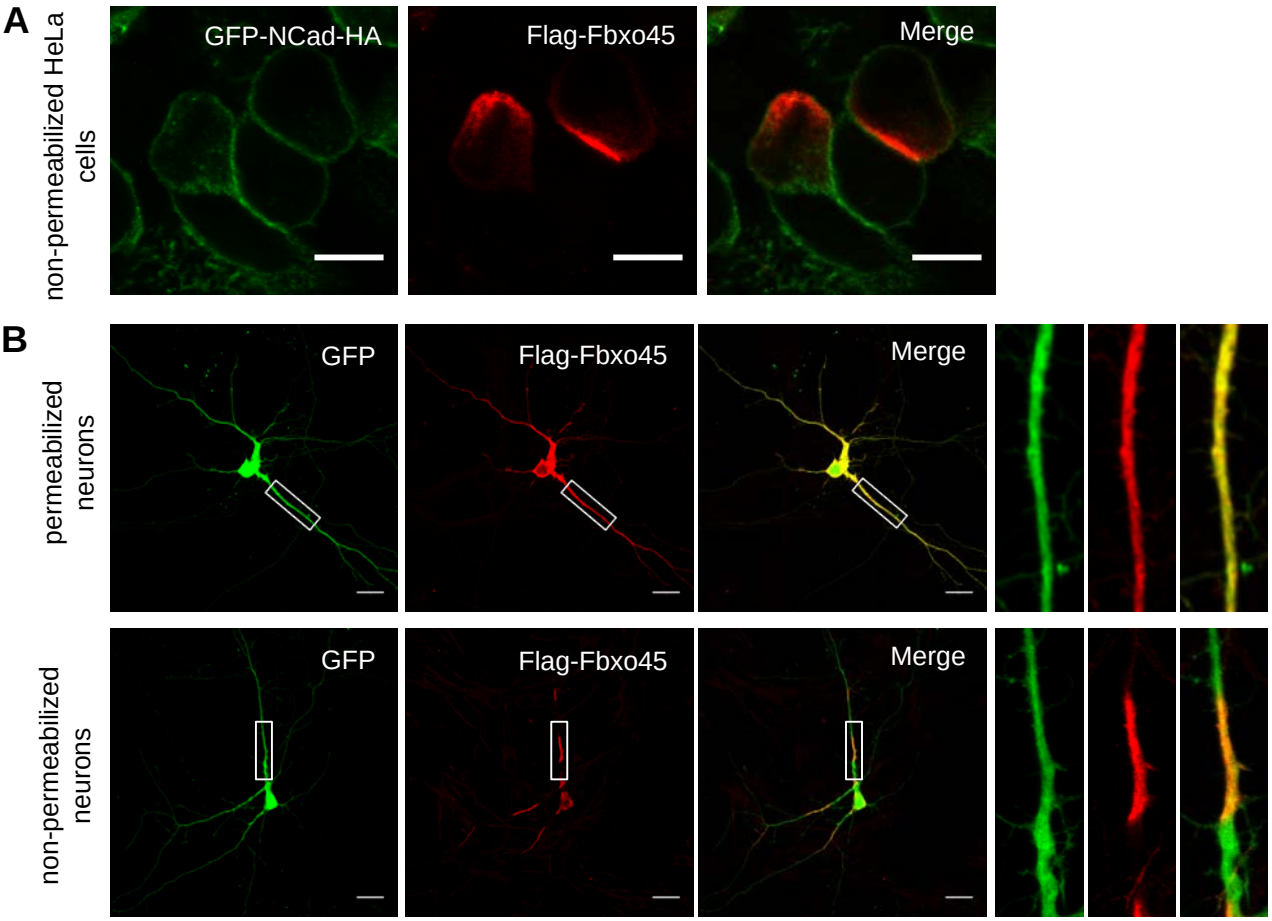
A
non-permeabilized HeLa cells
GFP-NCad-HA
Flag-Fbxo45
Merge
B
permeabilized neurons
GFP
Flag-Fbxo45
Merge
non-permeabilized neurons
GFP
Flag-Fbxo45
Merge

Figure 6

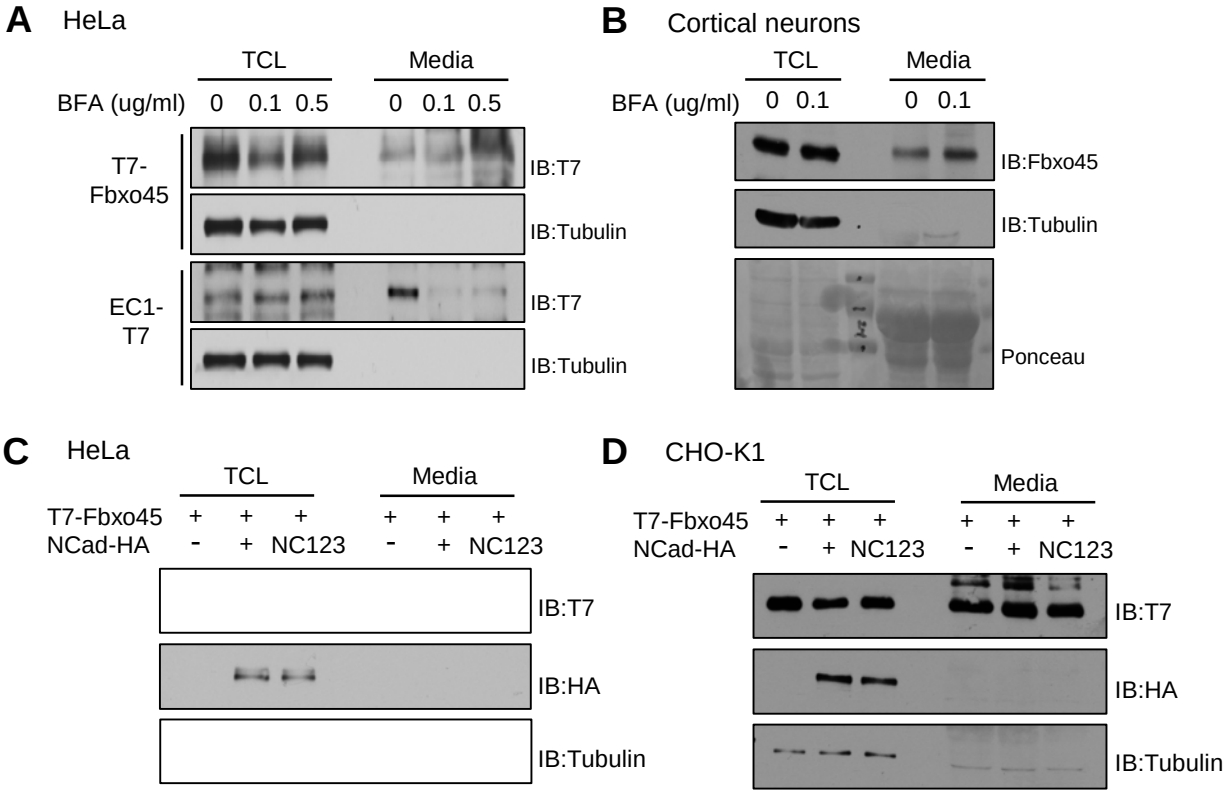
A
HeLa
TCL
Media
BFA (ug/ml) 0 0.1 0.5 0 0.1 0.5
T7-Fbxo45
IB:T7
IB:Tubulin
EC1-T7
IB:T7
IB:Tubulin
B
Cortical neurons
TCL
Media
BFA (ug/ml) 0 0.1 0 0.1
IB:Fbxo45
IB:Tubulin
Ponceau
C
HeLa
TCL
Media
T7-Fbxo45 + + + + + +
NCad-HA - + NC123 - + NC123
IB:T7
IB:HA
IB:Tubulin
D
CHO-K1
TCL
Media
T7-Fbxo45 + + + + + +
NCad-HA - + NC123 - + NC123
IB:T7
IB:HA
IB:Tubulin

Figure 7

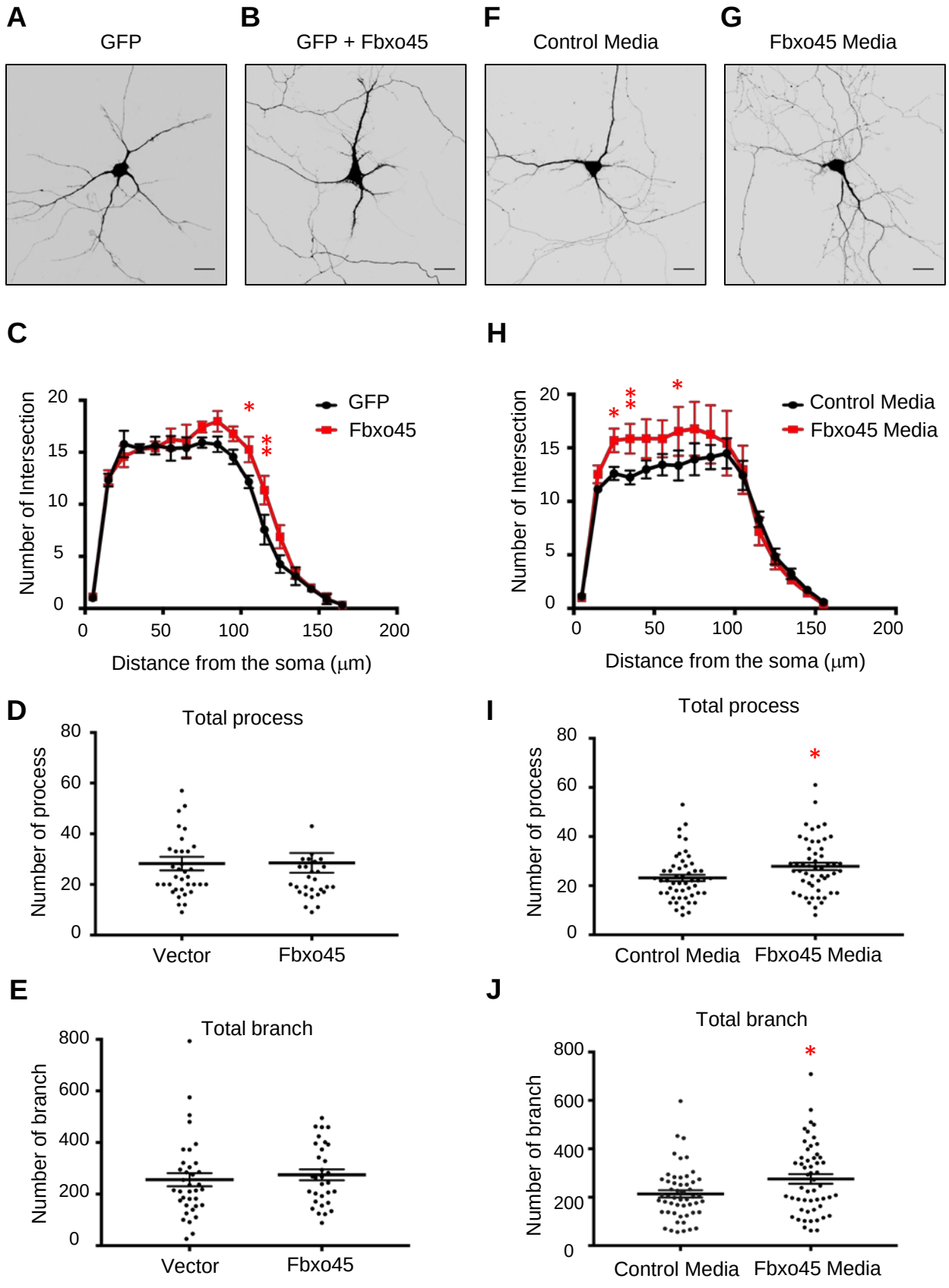
A
GFP
B
GFP + Fbxo45
F
Control Media
G
Fbxo45 Media
C
Number of Intersection
Distance from the soma (μm)
GFP
Fbxo45
H
Control Media
Fbxo45 Media
D
Total process
Number of process
Vector
Fbxo45
I
Total process
Control Media
Fbxo45 Media
E
Total branch
Number of branch
J
Total branch

Figure 8

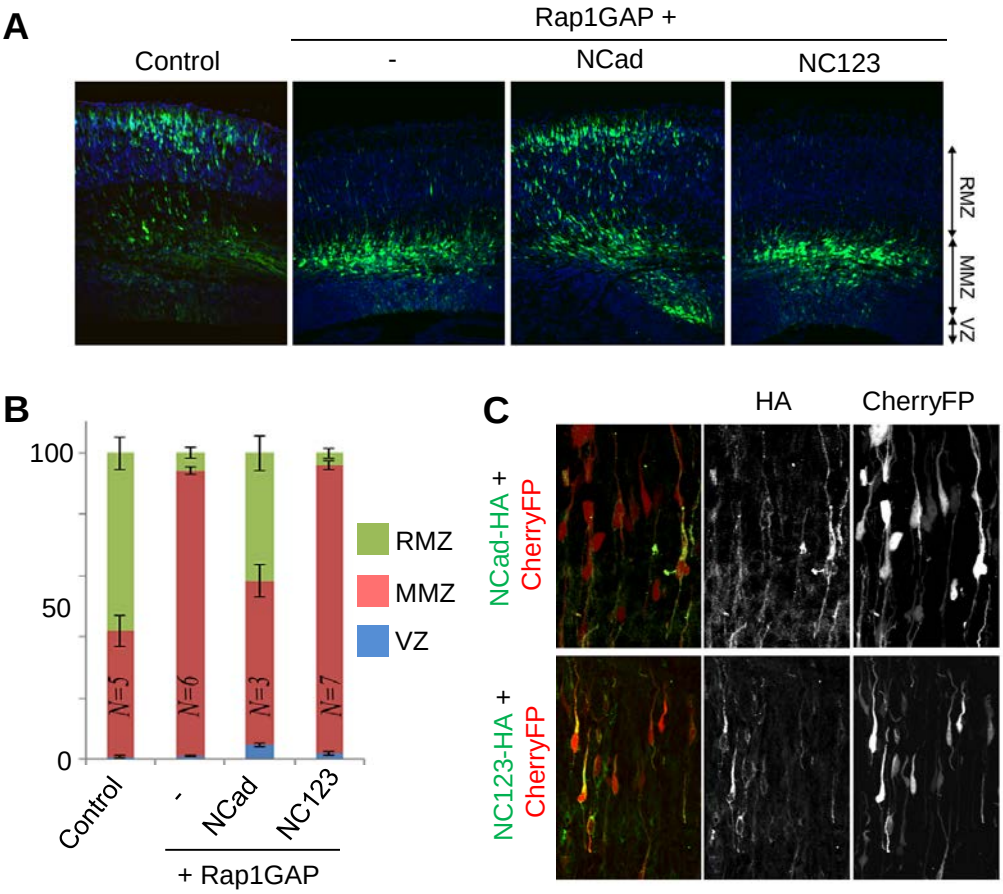
A
Rap1GAP +
Control
-
NCad
NC123
RMZ
MMZ
VZ
B
100
50
0
RMZ
MMZ
VZ
N=5
N=6
N=3
N=7
Control
-
NCad
NC123
+ Rap1GAP
C
HA
CherryFP
NCad-HA +
CherryFP
NC123-HA +
CherryFP

SUPPLEMENTARY TABLES

Supplementary Table 1. Rat proteins detected by BioID with NCad-BirA*.

Rat proteins detected by LC-MS/MS from two independent experiments. The numbers represent the score and the data was sorted by the score of N2-BirA* in experiment 2 as a descending manner. The score is the sum of all peptide Xcorr values above the specified score threshold. The score threshold is calculated as follows: 0.8 + peptide charge X peptide relevance factor. 0.4 was used for the peptide relevance factor. For each spectrum, only the highest-scoring match is used. Blank cells indicate that no peptide was detected in the sample.

Supplementary Table 2. Human proteins detected by BioID with NCad-BirA*.

Human proteins detected by mass spectrometry from the same two experiments as Table 1.

Supplementary Table 3. Mouse proteins detected by affinity purification as a binding candidate of NCad EC W161A.

Proteins from gel regions above and below of the cadherin-Fc bands in Figure 1F were digested with trypsin and analyzed by LC-MS/MS. The numbers represent the score calculated as described in Table 1. For each spectrum, only the highest-scoring match is used. Blank cells indicate that no peptide was detected in the sample.

Supplementary Table 1

Accession	Rat Gene	Protein description	Experiment 1			Experiment 2		
			GFP	N5-BirA*	N2-BirA*	E5-BirA*	N5-BirA*	N2-BirA*
D4A2D3	Mycbp2	Protein Mycbp2 (Fragment)	-	26.15	49.91	-	26.88	46.08
F1M8Q1	Fbxo45	F-box/SPRY domain-containing protein 1 (Fragment)	-	2.99	8.48	-	2.99	8.65
F1LYJ8	Gramd4	Protein Gramd4 (Fragment)	-	2.93	3.10	-	-	6.01
D3ZQN7	Lamb1	Protein Lamb1	-	-	8.00	-	-	5.51
F1LRM0	Scaper	Protein Scaper	-	-	2.13	-	2.51	5.50
P54777	Pex6	Peroxisome assembly factor 2	-	-	8.77	-	-	5.19
Q63362	Ndufa5	NADH dehydrogenase [ubiquinone] 1 alpha subcomplex subunit 5	-	2.67	-	-	-	3.38
O35796	C1qbp	Complement component 1 Q subcomponent-binding protein, mitochondrial	-	3.58	-	-	3.13	3.32
M0RB15	Rpp14	Uncharacterized protein	-	-	2.94	-	4.36	3.16
D3ZPE6	Mrpl51	Mitochondrial ribosomal protein L51 (Predicted)	-	-	3.47	-	3.34	2.94
B2GV24	Ufl1	E3 UFM1-protein ligase 1	-	2.48	-	-	2.19	2.93
F1LZW2	Dgkk	Diacylglycerol kinase (Fragment)	-	2.72	-	-	3.15	2.83
P36972	Aprt	Adenine phosphoribosyltransferase	-	3.38	-	-	-	2.69
P11951	Cox6c2	Cytochrome c oxidase subunit 6C-2	-	3.15	3.44	-	-	2.66
Q6P684	Smn1	Survival motor neuron 1	-	2.13	-	-	-	2.50
D3ZFF4	Lclat1	Protein Lclat1	-	-	6.21	-	1.82	2.46
F1LQE9	Ppp1r10	Uncharacterized protein	-	-	3.88	-	-	2.43
B2RZD2	Tmem126b	Complex I assembly factor TMEM126B, mitochondrial	-	2.32	-	-	3.18	2.27
Q3T1K9	Nicn1	Nicolin 1	-	-	3.18	-	0.00	2.23
Q6AYA1	Gar1	H/ACA ribonucleoprotein complex subunit 1	-	2.20	2.06	-	2.46	2.22
Q5BJS0	Dhx30	Putative ATP-dependent RNA helicase DHX30	-	-	2.41	-	2.04	2.11
D3ZI07	Kif3b	Kinesin-like protein	-	2.69	2.97	-	3.19	2.00
P50137	Tkt	Transketolase	-	10.03	7.29	-	2.59	-
D4ABT8	Hnrnpul2	Protein Hnrnpul2	-	7.52	7.17	-	2.01	-
M0R7U6	Sowahc	Protein Sowahc	-	3.16	3.90	-	2.72	-
F1MAF2	Akap17a	Protein Akap17a	-	3.17	3.29	-	3.59	-
D3ZHV9	Misp	Hypothetical LOC500797, isoform CRA_a	-	2.14	2.03	-	2.94	-
Q07009	Capn2	Calpain-2 catalytic subunit	-	3.10	-	-	2.65	-
D3ZZQ6	Ints4	Protein Ints4	-	2.18	-	-	2.53	-

Supplementary Table 2

Accession	Human Gene	Description	Experiment 1			Experiment 2		
			GFP	N5-BirA*	N2-BirA*	E5-BirA*	N5-BirA*	N2-BirA*
O75592-2	MYCBP2	Isoform 2 of Probable E3 ubiquitin-protein ligase MYCBP2	-	47.55	127.74	-	70.14	112.99
Q13751	LAMB3	Laminin subunit beta-3	-	-	2.71	-	-	8.56
Q9BR76	CORO1B	Coronin-1B	-	3.81	8.88	-	4.30	7.33
P46108-2	CRK	Isoform Crk-I of Adapter molecule crk	-	-	3.31	-	2.33	7.14
A6NJ11	UFD1L	Ubiquitin fusion degradation protein 1 homolog	-	3.12	3.33	-	8.55	5.86
Q9NT62-2	ATG3	Isoform 2 of Ubiquitin-like-conjugating enzyme ATG3	-	-	2.13	-	-	5.22
Q9Y3A6	TMED5	Transmembrane emp24 domain-containing protein 5	-	3.37	-	-	3.60	5.19
Q5SSJ5-3	HP1BP3	Isoform 3 of Heterochromatin protein 1-binding protein 3	-	2.96	3.59	-	0.00	5.16
Q15750-2	TAB1	Isoform 2 of TGF-beta-activated kinase 1 and MAP3K7-binding protein 1	-	-	3.50	-	2.15	4.38
B4DEK4	SNX2	Sorting nexin-2	-	4.88	2.84	-	5.53	4.25
Q8TCG1-2	KIAA1524	Isoform 2 of Protein CIP2A	-	3.70	4.30	-	-	3.65
Q09472	EP300	Histone acetyltransferase p300	-	3.18	2.44	-	-	3.34
Q9UHI6	DDX20	Probable ATP-dependent RNA helicase DDX20	-	-	2.52	-	3.70	3.18
O95400	CD2BP2	CD2 antigen cytoplasmic tail-binding protein 2	-	3.61	6.02	-	3.20	3.07
Q9UHG3	PCYOX1	Prenylcysteine oxidase 1	-	-	5.62	-	-	2.80
P11047	LAMC1	Laminin subunit gamma-1	-	-	22.15	-	-	2.80
J3KRS1	DHRS7B	Dehydrogenase/reductase SDR family member 7B (Fragment)	-	2.78	3.79	-	-	2.78
O15063	KIAA0355	Uncharacterized protein KIAA0355	-	2.90	2.63	-	5.67	2.77
P67775-2	PPP2CA	Isoform 2 of Serine/threonine-protein phosphatase 2A catalytic subunit alpha isoform	-	1.66	1.90	-	-	2.70
B4DT16	BCL11A	B-cell lymphoma/leukemia 11A	-	2.37	-	-	-	2.69
E7ERI3	TARS	Threonine--tRNA ligase, cytoplasmic	-	1.92	-	-	2.73	2.63
Q70E73-5	RAPH1	Isoform RMO1c of Ras-associated and pleckstrin homology domains-containing protein 1	-	-	4.16	-	-	2.60
O76024	WFS1	Wolframin	-	-	2.60	-	2.29	2.51
D6REK3	CWC27	Peptidyl-prolyl cis-trans isomerase CWC27 homolog	-	-	2.51	-	-	2.50
O14617-4	AP3D1	Isoform 4 of AP-3 complex subunit delta-1	-	-	0.00	-	2.61	2.46
Q99848	EBNA1BP2	Probable rRNA-processing protein EBP2	-	-	1.94	-	1.83	2.44
H0Y380	PTPRF	Receptor-type tyrosine-protein phosphatase F (Fragment)	-	-	2.38	-	2.07	2.16
Q9UL03-3	INTS6	Isoform 3 of Integrator complex subunit 6	-	2.47	3.12	-	-	2.15
O75382-4	TRIM3	Isoform 4 of Tripartite motif-containing protein 3	-	-	3.98	-	-	2.12
M0QYC5	SIN3B	Paired amphipathic helix protein Sin3b	-	-	3.68	-	3.63	2.08
H3BPL5	CCDC101	SAGA-associated factor 29 homolog	-	-	2.50	-	2.06	2.06
Q9H944	MED20	Mediator of RNA polymerase II transcription subunit 20	-	-	3.32	-	-	2.03
Q8ND04	SMG8	Protein SMG8	-	4.56	-	-	-	2.01
Q9H061	TMEM126A	Transmembrane protein 126A	-	2.76	-	-	3.52	-
P08621-2	SNRNP70	Isoform 2 of U1 small nuclear ribonucleoprotein 70 kDa	-	5.10	3.18	-	1.79	-
J3KQN6	PPP2R5E	Serine/threonine-protein phosphatase 2A 56 kDa regulatory subunit epsilon isoform	-	4.01	4.50	-	2.38	-
E9PGB5	SFXN4	Sideroflexin-4	-	2.02	1.64	-	1.72	-
Q0PRL4	FOXP2	Forkhead box P2 variant 3	-	3.39	-	-	3.02	-
H7C0X5	CPVL	Probable serine carboxypeptidase CPVL (Fragment)	-	2.39	2.23	-	2.07	-
E9PM04	DCUN1D5	DCN1-like protein	-	3.43	-	-	2.87	-
F5GXS7	METAP1	Methionine aminopeptidase	-	2.80	4.69	-	2.07	-
F5H6N1	MAGOHB	Protein mago nashi homolog 2	-	3.09	3.03	-	2.66	-
K7EKI4	MRPL4	39S ribosomal protein L4, mitochondrial	-	2.48	-	-	2.09	-
S4R432	CBWD3	COBW domain-containing protein 3 (Fragment)	-	7.27	-	-	1.99	-
Q5H937	PKIG	cAMP-dependent protein kinase inhibitor gamma	-	-	3.10	-	1.89	-
E7EN38	RAD50	DNA repair protein RAD50 (Fragment)	-	-	3.47	-	3.78	-
Q7Z2Z2-2	EFTUD1	Isoform 2 of Elongation factor Tu GTP-binding domain-containing protein 1	-	-	2.81	-	1.85	-
B3KT28	FAF1	FAS-associated factor 1	-	-	2.27	-	2.29	-
B4DVY7	FLOT1	Flotillin-1	-	-	4.30	-	2.58	-
D6RBM3	CASP6	Caspase-6 subunit p18	-	-	3.13	-	2.75	-
P09496-5	CLTA	Isoform 5 of Clathrin light chain A	-	-	7.16	-	4.60	-
F5GX19	LAMTOR1	Ragulator complex protein LAMTOR1	-	-	2.70	-	2.55	-

Supplementary Table 3

Accession	Gene	Description	Ecad-Fc	Ncad^{W161A}-Fc
Q7TPH6-2	Mycbp2	Isoform 2 of Probable E3 ubiquitin-protein ligase MYCBP2	-	205.37
Q8K3B1	Fbxo45	F-box/SPRY domain-containing protein 1	-	27.50
Q8R1J9	Tor2a	Torsin-2A	-	21.99
Q8C570	Rae1	mRNA export factor	-	13.51
O88838	Spsb2	SPRY domain-containing SOCS box protein 2	-	12.70
P83940	Tceb1	Transcription elongation factor B polypeptide 1	-	10.66
Q9D051	Pdhb	Pyruvate dehydrogenase E1 component subunit beta, mitochondrial	-	9.71
Q9WTX5	Skp1	S-phase kinase-associated protein 1	-	7.54
Q9DCL9	Paics	Multifunctional protein ADE2	-	7.10
A2A5N1	Ywhab	14-3-3 protein beta/alpha (Fragment)	-	6.49
Q9CZU6	Cs	Citrate synthase, mitochondrial	-	6.22
O08573-2	Lgals9	Isoform Short of Galectin-9	-	5.36
E9Q9B3	Spryd3	Protein Spryd3	-	5.31
Q61830	Mrc1	Macrophage mannose receptor 1	-	5.23
Q61753	Phgdh	D-3-phosphoglycerate dehydrogenase	-	4.98
P11983-2	Tcp1	Isoform 2 of T-complex protein 1 subunit alpha	-	4.90
Q8BM88	Ctso	Cathepsin O	-	4.48
Q6P5E4	Uggt1	UDP-glucose:glycoprotein glucosyltransferase 1	-	3.69
F8WJ41	Rps15a	40S ribosomal protein S15a (Fragment)	-	3.56
H3BJB6	Cct8	T-complex protein 1 subunit theta (Fragment)	-	2.99
P59708	Sf3b14	Pre-mRNA branch site protein p14	-	2.97
Q9JJV2-3	Pfn2	Isoform 3 of Profilin-2	-	2.71
G3UXF3	Cct4	T-complex protein 1 subunit delta	-	2.70
P56379	Mp68	6.8 kDa mitochondrial proteolipid	-	2.56
G3UZJ2	Map2	Microtubule-associated protein (Fragment)	-	2.53
H7BX22	Ranbp1	Ran-specific GTPase-activating protein	-	2.52
P99027	Rplp2	60S acidic ribosomal protein P2	-	2.51
D3YVF4	Rps14	40S ribosomal protein S14 (Fragment)	-	2.43
Q99J74	Tusc3	Tumor suppressor candidate 3	-	2.25
P55284	Cdh5	Cadherin-5	-	2.15
E0CZA1	Cct5	T-complex protein 1 subunit epsilon (Fragment)	-	2.14
E9Q0W8	Snrpe	Small nuclear ribonucleoprotein E	-	2.09
Q9CZM3	Tmem33	Transmembrane protein 33	-	2.07
Q9Z0F5	Ch25h	Cholesterol 25-hydroxylase	-	2.06
Q60692	Psmb6	Proteasome subunit beta type-6	-	2.01
P00493	Hprt1	Hypoxanthine-guanine phosphoribosyltransferase	-	2.00
P62077	Timm8b	Mitochondrial import inner membrane translocase subunit Tim8 B	-	1.99
Q07646-2	Mest	Isoform 2 of Mesoderm-specific transcript protein	-	1.96
Q3UEG7	Itih2	Inter-alpha-trypsin inhibitor heavy chain H2 (Fragment)	-	1.84
Q9DCC4	Pycrl	Pyrroline-5-carboxylate reductase 3	-	1.80
E9Q3T0	Gm10073	Uncharacterized protein	-	1.78
P01029	C4b	Complement C4-B	-	1.77
Q6P5D8	Smchd1	Structural maintenance of chromosomes flexible hinge domain-containing protein 1	-	1.73
A2A7B3	Spsb1	SPRY domain-containing SOCS box protein 1 (Fragment)	-	1.73
Q91V01	Lpcat3	Lysophospholipid acyltransferase 5	-	1.70
Q6P069-2	Sri	Isoform 2 of Sorcin	-	1.69
Q3V1Z5	Rps4l	Protein Rps4l	-	1.60

SUPPLEMENTARY FIGURE LEGENDS

Supplementary Figure 1, related to Figure 1.

Controls for BioID and affinity purification mass spectrometry.

(A) NCad or cadherin-BirA* fusion proteins were expressed in HeLa cells and incubated with or without biotin. Cell lysates were collected and blotted with HA or Myc antibodies or strepavidin as indicated. (B) Low power images of Figure 1A. Enlarged images of the inner square were shown in Figure 1A. Scale bar: 20 μm. (C) Preparative SDS polyacrylamide gel used for protein identification by affinity chromatography. The lanes correspond to samples 8, 9 (duplicate lanes), 11 (duplicate lanes) and 10 of Figure 2A. The gel was stained with colloidal Coommassie Blue (Simple Blue, BioRad). The boxes indicate regions excised for protein identification by LC-MS/MS.

Supplementary Figure 2, related to Figure 4.

NC123 mutant supports homophilic interaction.

(A) Quantification of replicate CHO-K1 aggregation assays shown in Figure 4D. N_0: particle number at time 0 min, N_{20}: particle number at time 20 min. n = 6. ***p <0.001.

(B) Aggregation assay with two different cell populations to investigate trans-interaction between NCad wildtype and mutants. Green cells, co-expressing NCad wildtype and GFP, were mixed with red cells, co-expressing NCad wildtype or mutants and mCherry. Scale bar: 400 μm.

Supplementary Figure 3, related to Figure 5.

Sub-cellular localization of Fbxo45.

(A) Low power images of non-permeabilized HeLa cells. Enlarged images of the inner square were shown in Figure 5A. Scale bar: 20 μm. (B-C) GFP-NCad and Flag-Fbxo45 were co-transfected and immunofluorescence was performed using Flag antibody after permeabilization.

(B) HeLa cells. Enlarged images of the inner square were shown in the bottom row. Scale bar: top row, 20 μm; bottom row, 10 μm. (C) Mouse hippocampal neurons. Scale bar: 20 μm.

Supplementary Figure 4, related to Figure 7.

Secreted Fbxo45 did not change dendritic arborization during DIV 1 to 3.

(A-F) Additional data for Figure 7. (A, B) Flag-Fbxo45 immunostaining of Figure 7A and B, respectively. Scale bar: 20 μm. Total neurite outgrowth and mean process lengths were compared in Fbxo45 overexpression (C, D) and secreted Fbxo45 (E, F). Error bar shows mean ± S.E.M. of three (C, D) and five (E, F) biologically independent experiments.

(G-M) Data for the neurons transfected with GFP or GFP and Flag-Fbxo45 on DIV1 and visualized on DIV3. (G, H) Representative GFP images to show the dendritic arborization. Scale bar: 20 μm. (I) Sholl analysis. Error bar shows mean ± S.E.M. of four biologically independent experiments. (J) Total neurite number. (K) Total branch numbers. (L) Total neurite outgrowth. (M) Mean process lengths.

Supplementary Figure 5, related to Figure 8.

Over-expression of Fbxo45 slows neuron migration.

(A) Representative images to show the positions of electroporated cells at E17.5. Embryos were electroporated with mCherry alone or together with Fbxo45. mCherry, red; DAPI, blue. Scale bar: 100 μm. The cerebral cortex was subdivided into radial morphology zone (RMZ; cortical plate and upper intermediate zone), multipolar morphology zone (MMZ; middle and lower intermediate zone and subventricular zone (SVZ)) and ventricular zone (VZ). (B) Percentage of electroporated cells in each zone (n=4 control, n=2 Fbxo45).

Supplementary Figure 1

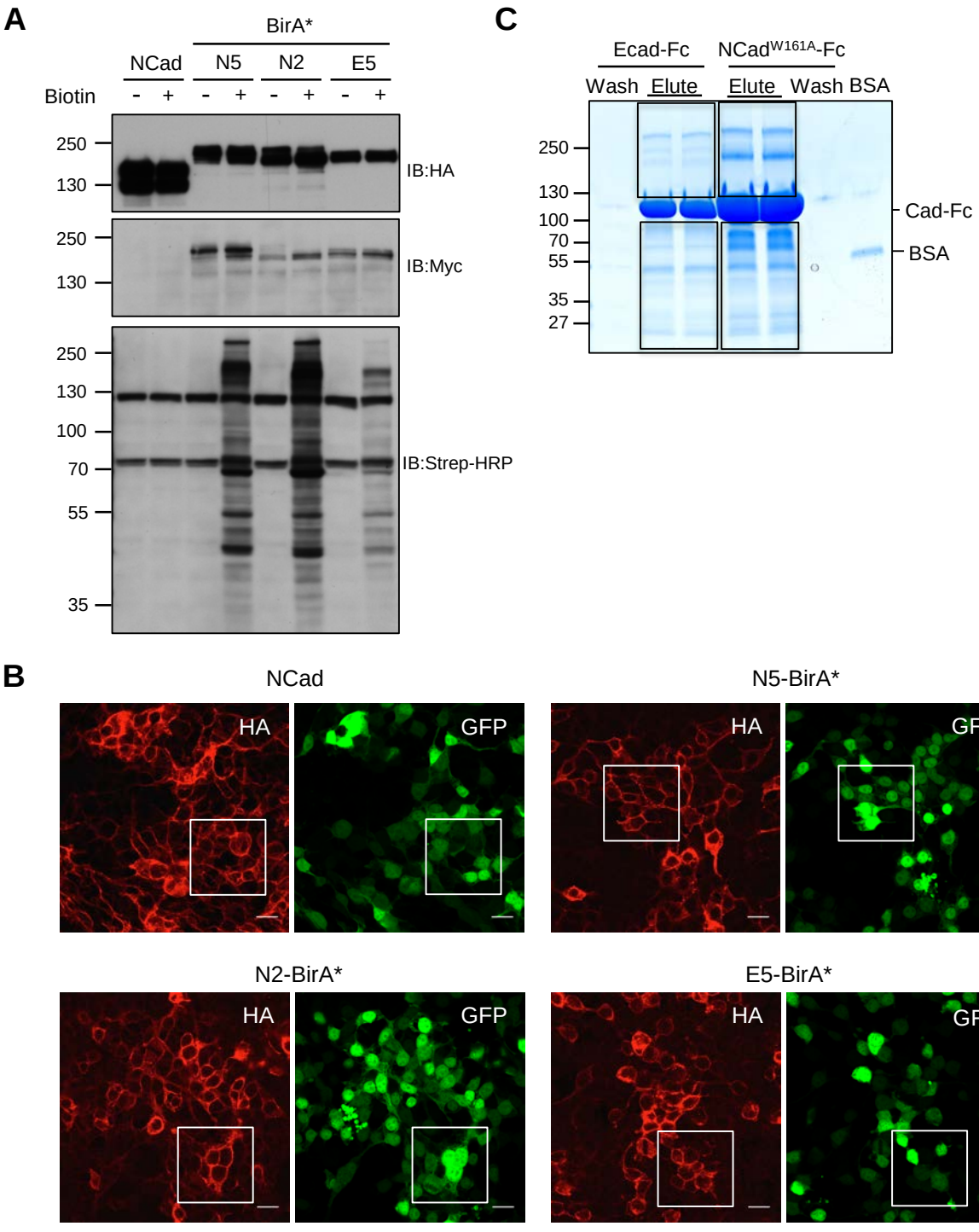

Supplementary Figure 2

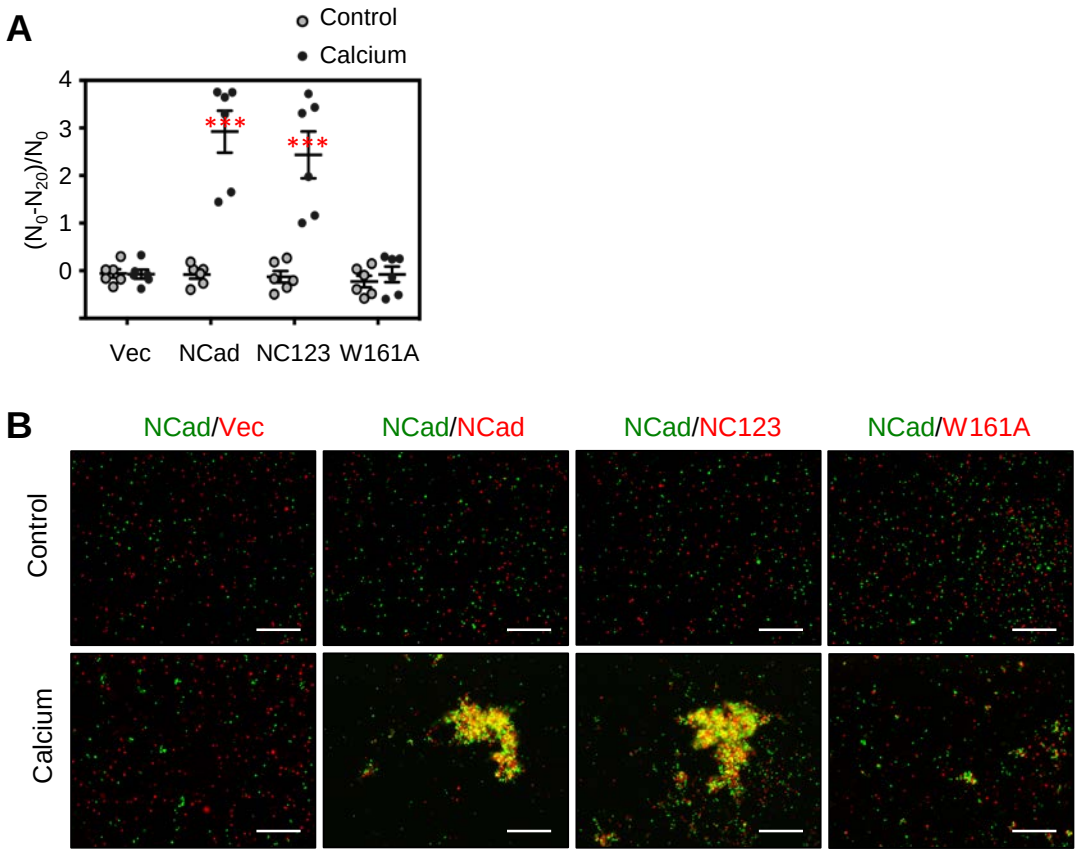

Supplementary Figure 3

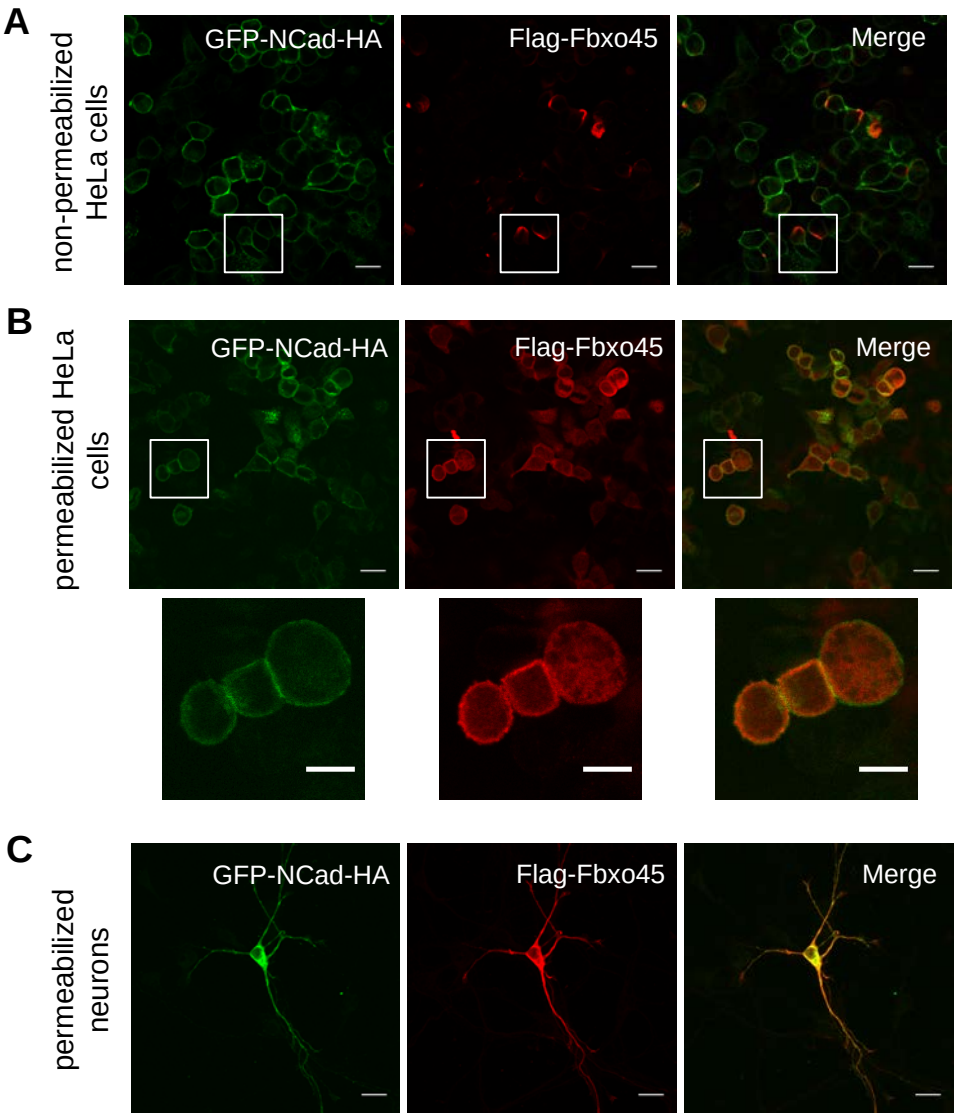

Supplementary Figure 4

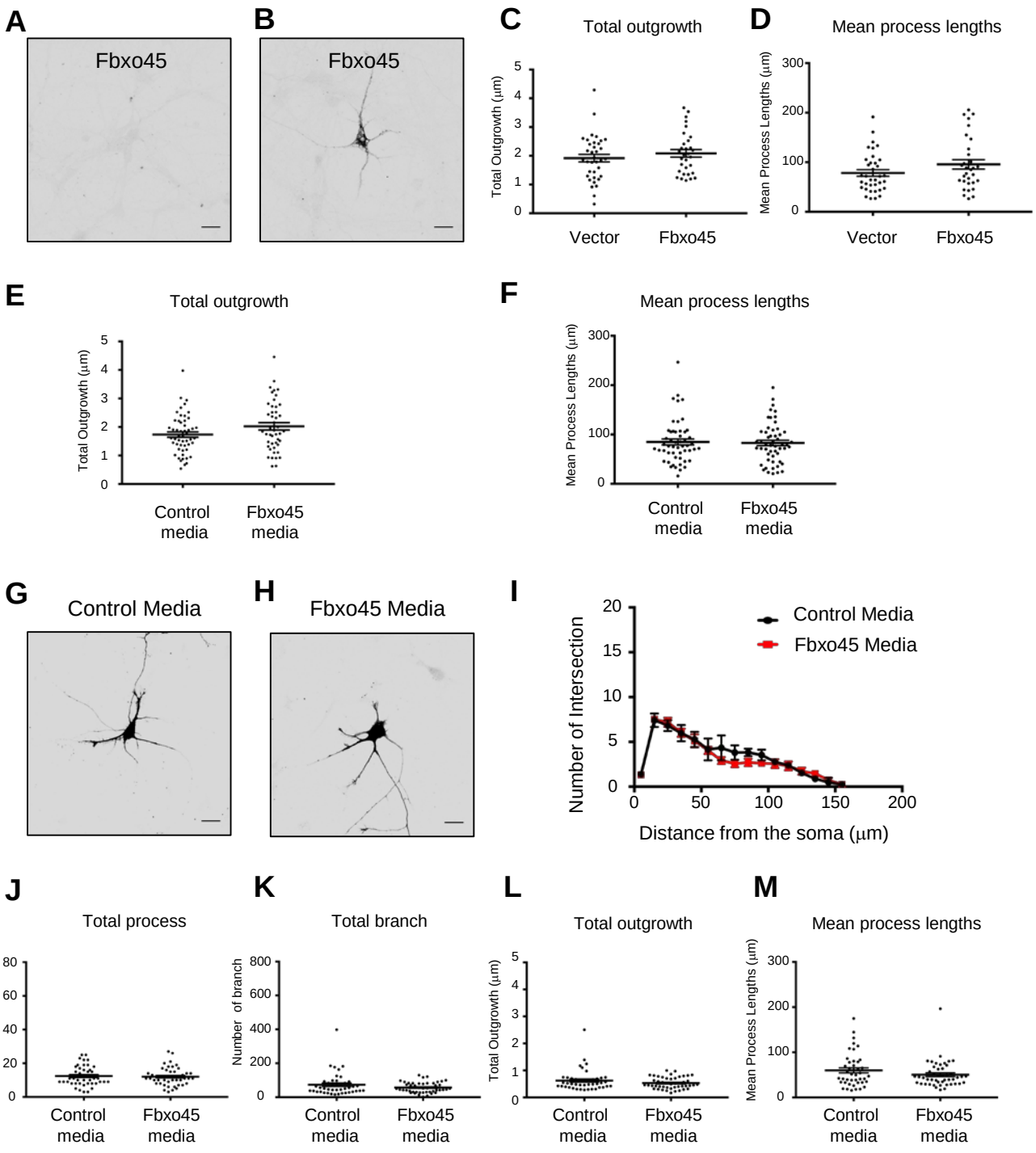

Supplementary Figure 5